Characterisation and diachronous initiation of coarse clastic deposition in the Magallanes–Austral foreland basin, Patagonian Andes

Matthew A. Malkowski,* Glenn R. Sharman,† Stephan A. Graham* and Andrea Fildani‡

*Department of Geological Sciences, Stanford University, Stanford, CA, USA
†ConocoPhilips Exploration & Production, Houston, TX, USA
‡Statoil Research Center, Austin, TX, USA

ABSTRACT

Magallanes–Austral Basin (MAB) fill is preserved along a >1000 km north–south trending outcrop belt in the southern Patagonia region of Argentina and Chile. Although the stratigraphic evolution of the MAB has been well documented in the Chilean sector (referred to as the Magallanes Basin), its northern terminus in southern Argentina (Austral Basin) is poorly constrained. We present new stratigraphic and geochronologic analyses of the early basin fill (Aptian–Turonian) from the Argentine sector (49–51°S) of the MAB to document spatial variability in stratigraphy and timing of deposition during the initial stages of basin evolution. The initiation of the retroarc foreland basin fill is marked by the transition from mudstone to coarse-clastic deposition, which is characterised by the consistent presence of sandstone beds > *ca.* 20 cm thick interpreted to represent sediment gravity flows deposited in a submarine fan system. Depositional environments within the early fill of the basin range from lower to upper deep-water fan settings as well as previously undocumented slope deposits. These facies are present as far north as El Chalten, Argentina (*ca.* 49°S), indicating that facies-equivalent rocks can be traced along-strike for at least 5 degrees of latitude, based on correlation with strata as far south as the Cordillera Darwin (*ca.* 54°S). Eight new U-Pb zircon ages from ash beds reveal an overall southward younging trend in the initiation of coarse clastic deposition. Inferred depositional ages range from *ca.* 115 ± 1.9 Ma in the northernmost study area to not older than 92 ± 1 Ma and 89 ± 1.5 Ma in the central and southern sectors respectively. The apparent diachronous delivery of coarse detritus into the basin may reflect (1) gradual southward progradation of a deep-water fan system from a northerly point source and/or (2) orogen-parallel variations in the timing and magnitude of thrust-belt deformation and erosion that provided more local sources for sediment delivery.

INTRODUCTION

Retroarc foreland basins are commonly characterised as crustal depressions that develop over continental crust between an orogenic belt and the craton (Dickinson, 1974; Beaumont, 1981; DeCelles & Giles, 1996). These *continental* foreland basins often initiate with shallow- to nonmarine depositional systems and quickly develop accommodation–limited conditions and become overfilled, which results in dominantly transverse sediment dispersal systems (Fig. 1a) (Heller *et al.*, 1988; Jordan, 1995; DeCelles & Giles, 1996; Horton & DeCelles, 1997; Leier *et al.*, 2007; Szwarc *et al.*, 2014). In contrast, some retroarc foreland basins develop over rifted or attenuated crust incorporating inherited structures and variations in crustal properties (e.g. rheology, density, elasticity, etc.),

which have been described as 'successor' foreland basins (cf. Graham *et al.*, 1993; Fosdick *et al.*, 2014). This inheritance can profoundly influence how foreland basin systems evolve both structurally and stratigraphically (Stockmal *et al.*, 1986; Desegaulx *et al.*, 1991; Romans *et al.*, 2010; Fosdick *et al.*, 2014). For instance, successor foreland basin systems that initiate on attenuated crust are more prone to enhanced subsidence that results in long-lived, underfilled basin conditions and a protracted phase of deep-marine deposition that utilises a principally longitudinal (axial) sediment dispersal system (Fig. 1b) (e.g. Romans *et al.*, 2010, 2011). In addition, the influence of weakened crust and thick sediment overburden leads to enhanced crustal flexure in the foreland and thus broader deflection towards the craton, which results in a subdued forebulge zone (Fosdick *et al.*, 2014).

Although the stratigraphic evolution of continental foreland basins is relatively well documented (e.g. Heller *et al.*, 1988; Gardner, 1995; Jordan, 1995; Schwans, 1995; DeCelles & Giles, 1996; Wang *et al.*, 2013), that of suc-

Correspondence: Matthew A. Malkowski, 450 Serra Mall, Building 320, Stanford, CA 94305, USA. E-mail: mamalkow@stanford.edu
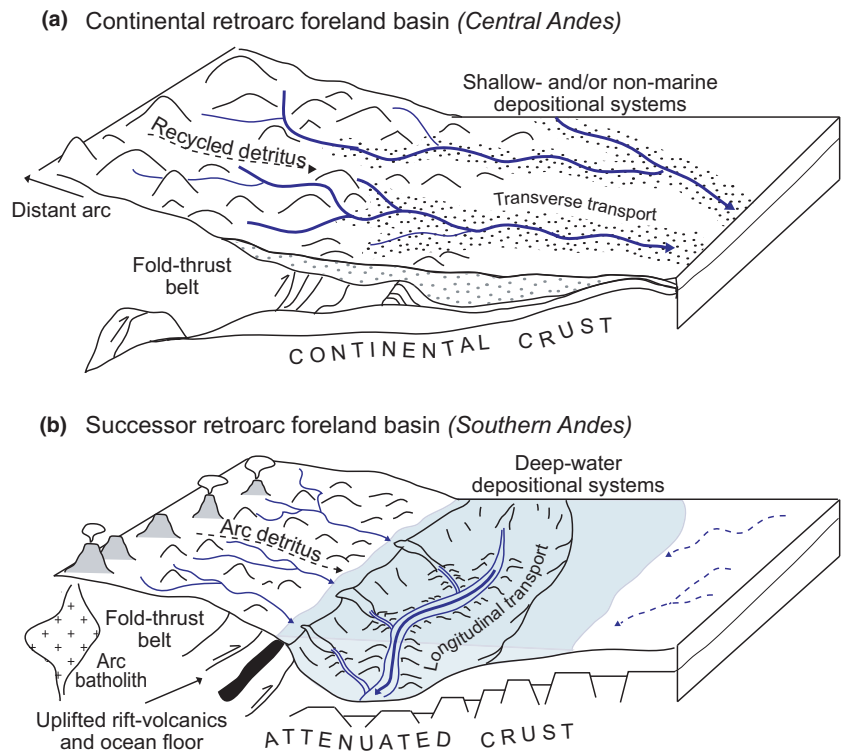
(a) Continental retroarc foreland basin *(Central Andes)*

(b) Successor retroarc foreland basin *(Southern Andes)*

Fig. 1. Schematic diagrams showing some of the structural and stratigraphic characteristics of two different types of retroarc foreland basin systems: (a) continental retroarc foreland basin (after Horton & DeCelles, 1997) such as that found in the Cenozoic Central Andes, and (b) successor retroarc foreland basin (after Romans *et al.*, 2010 and Fosdick *et al.*, 2014), which is more characteristic of the Cretaceous–Paleogene southernmost Andes.

cessor foreland basin systems remains somewhat underrepresented in the literature despite an abundance of examples (e.g. Aquitaine Basin, Austrian Molasse Basin, Ebro Basin, Magallanes–Austral Basin) (cf. Desegaulx *et al.*, 1991; Wilson, 1991; Puigdefàbregas *et al.*, 1992; Fildani & Hessler, 2005; De Ruig & Hubbard, 2006). This investigation adds to a growing body of knowledge about successor foreland basins by characterising the depositional facies, stratigraphic architecture and timing of deposition during the early phases of the Magallanes–Austral retroarc foreland basin (Fig. 2). In addition, this work constrains the initial basin evolution and palaeogeography of the Cretaceous foreland basin near the southernmost Andes.

The Late Cretaceous Magallanes–Austral Basin (MAB) of southern Patagonia is preserved along a nearly continuous (>1000 km) north–south trending outcrop belt of Cretaceous–Paleogene stratigraphy in the foothills of the southernmost Andes (Fig. 2) and is a well-preserved example of a successor retroarc foreland basin system. The Mesozoic history of the region is characterised by basin inversion from an early extensional phase (Rocas Verdes backarc basin) to a subsequent contractile phase (Magallanes–Austral retroarc foreland basin) associated with Andean orogenesis (Wilson, 1991; Fildani & Hessler, 2005). This study presents new U-Pb zircon geochronology and detailed sedimentological and stratigraphic data from the relatively poorly known northern (Austral) sector of the MAB (Fig 2). Combined with previous studies, this work documents the basin-scale distribution and variability in the timing of deposition and depositional facies during the early stages of foreland basin fill. Our results

reveal a diachronous (southward younging) initiation of deposition by sediment gravity flows along one or more deep-water fan systems from as far north as El Chalten (*ca.* 49°S) to at least as far south as the Cordillera Darwin (*ca.* 55°S). This work also shows that temporal and spatial variations in depositional setting and sediment distribution correspond to along-strike crustal variations that were inherited prior to development of a foreland basin system. This reinforces the notion that crustal inheritance exerts an important and fundamental control on the stratigraphic evolution of foreland basins.

GEOLOGIC BACKGROUND

Basin evolution

The Jurassic–Neogene basin evolution of southern Patagonia consists of a two-phase history, which includes an older backarc rift phase (the Rocas Verdes Basin) and a subsequent retroarc foreland basin (Magallanes–Austral Basin) (Fig. 2) (Wilson, 1991; Fildani & Hessler, 2005; Calderón *et al.*, 2007; Romans *et al.*, 2010). A backarc extensional setting (the Rocas Verdes Basin) associated with the break-up of Gondwana characterised the southern Patagonian Andes region of South America during Jurassic – Early Cretaceous time (Katz, 1963; Dalziel *et al.*, 1974; De Wit & Stern, 1981; Biddle *et al.*, 1986). Lithospheric extension is recorded through bimodal volcanism including basalt and gabbro of the Sarmiento and Tortuga ophiolite complexes, and widespread silicic volcanism of the El Quemado, Ibañez and Tobífera Formations of western Patagonia (Fig. 2) (Saunders *et al.*, 1979;
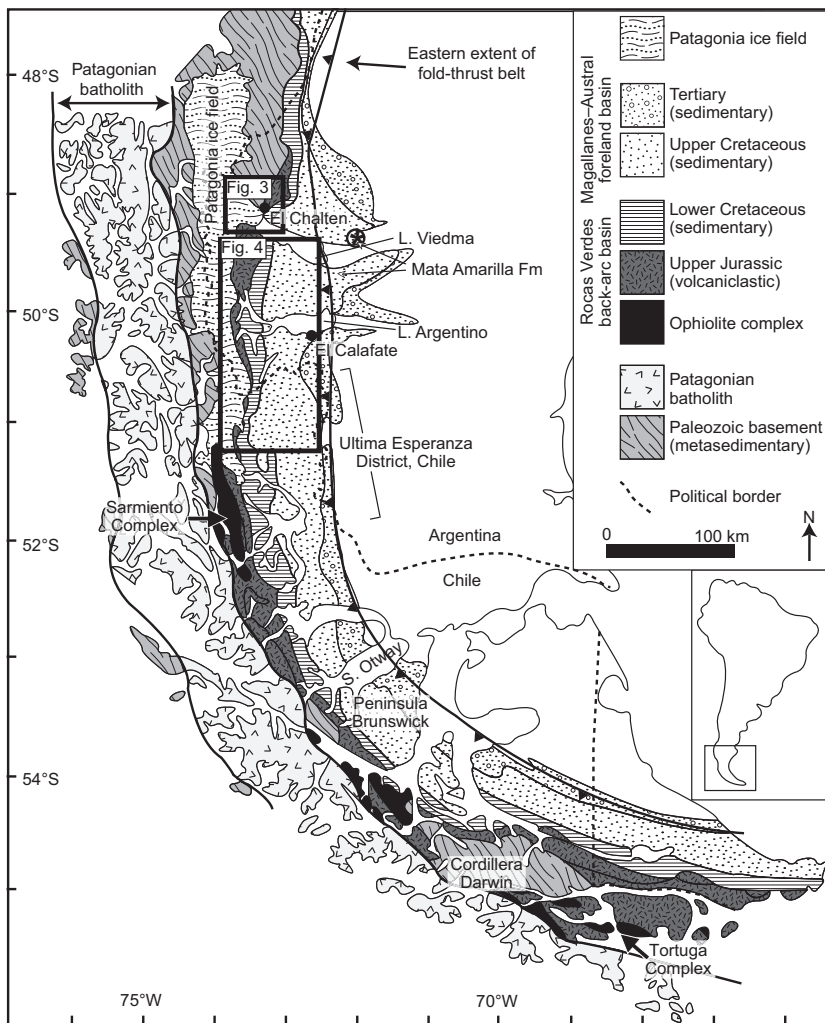
Fig. 2. Geologic map of southern Patagonia highlighting Jurassic–Cretaceous volcanic and sedimentary rocks associated with the Jurassic Rocas Verdes back-arc and the Cretaceous retroarc foreland fold-and-thrust belt. Modified from Biddle *et al.* (1986), Wilson (1991) and Fildani & Hessler (2005). Asterisk corresponds to approximate location of tuff age from Varela *et al.* (2012), see text for explanation.

De Wit & Stern, 1981; Pankhurst *et al.*, 2000; Calderón *et al.*, 2007). The resulting syn-rift Rocas Verdes Basin was filled by volcaniclastic units associated with the silicic volcanics mentioned above, and by black shale of the Rio Mayer and Zapata Formations in Argentina and Chile respectively (Wilson, 1991; Fildani & Hessler, 2005; Richiano, 2014).

The transition from backarc extension to compression is recorded by flexural deepening of the foredeep from 100–500 m water depth during the Aptian–Albian time up to 1000–2000 m by Albian–Cenomanian time (Natland *et al.*, 1974). The formation of a fully developed foreland basin is represented by the onset of deep-marine coarse clastic deposition of the Punta Barrosa Formation (Wilson, 1991; Fildani *et al.*, 2003; Fildani & Hessler, 2005) (Fig. 3). The presence of inherited, attenuated crust related to the early extensional phase allowed for prolonged deep-water sedimentation (Fildani & Hessler, 2005; Romans *et al.*, 2010, 2011). Continued evolution of the foreland basin resulted in a deep-marine axial channel belt that delivered sediment diachronously from north to south, as recorded by the Cerro Toro Formation (Winn & Dott, 1979; Crane & Lowe, 2008; Hubbard *et al.*, 2008; Jobe *et al.*, 2010; Bernhardt *et al.*, 2012). This, in turn, is

overlain by the Tres Pasos Formation, which reflects southward progradation of the deep-marine slope (Schultz *et al.*, 2005; Hubbard *et al.*, 2008; Armitage *et al.*, 2009; Romans *et al.*, 2009) . Finally, deep-marine facies transition upward to shallow- and marginal-marine deposits of the uppermost Cretaceous Dorotea Formation (Covault *et al.*, 2009; Romans *et al.*, 2011; Schwartz & Graham, 2014).

Punta Barrosa formation

Nomenclature

Consensus in the stratigraphic nomenclature for the MAB outcrops has been hindered by inconsistency in naming formations across national borders (Fig. 3). The usage of the 'Punta Barrosa Formation' has been previously restricted to the Chilean sector of the basin (Magallanes Basin) in the Ultima Esperanza District, and has not been assigned to any stratigraphy from the Argentine basin sector (Austral Basin). For the purposes of this study, we extend the Punta Barrosa Formation nomenclature to refer to stratigraphy that represents the first consistent appearance of coarse-clastic deposition (e.g.
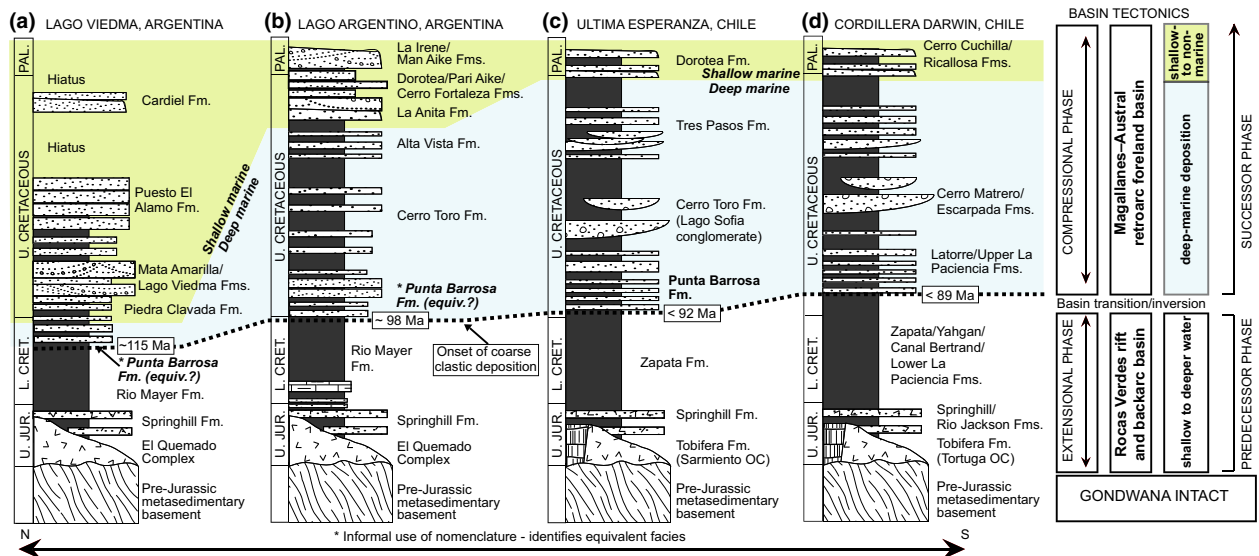
Fig. 3. Generalised stratigraphic correlations between units exposed along-strike (N–S) of the Patagonia fold-and-thrust belt. Data from this study combined with previous workers show a southward younging trend in the onset of coarse clastic deposition. Blue-shaded region corresponds to deep-water deposition and green shaded region corresponds to shallow- and nonmarine deposition. Generalised stratigraphy of: (a) the region just north of Lago Viedma (near El Chalten) in Argentina, modified after Arbe (2002); (b) the region just north of Lago Argentinto in Argentina, modified after Kraemer & Riccardi (1997); (c) the Ultima Esperanza district of southern Chile, modified after Wilson (1991), Fildani & Hessler (2005) and Romans *et al.* (2010); and (d) the Cordillera Darwin region in Chile, modified after McAtamney *et al.* (2011).

medium-grained sandstone) associated with turbiditic, deep-water facies, as defined by previous workers (e.g. Wilson, 1991; Fildani *et al.*, 2003; Fildani & Hessler, 2005). Most notably, this nomenclature expansion includes the Austral Basin, where it has been previously mapped and referred to as undifferentiated units of the Cerro Toro Formation (near Lago Argentino) (Arbe & Hechem, 1984) and in some cases the Rio Mayer formation (near Lago Viedma) (Kosmal & Spikermann, 2001). We correlated across national boundaries on the basis of mapping and tracing the continuation of facies-equivalent strata and key surfaces and stratigraphic packages along the outcrop belt (Fig. 3). South of the Ultima Experanza district of Chile, near the Cordillera Darwin, the Punta Barrosa facies equivalent rocks are referred to as the Latorre and/or Upper La Paciencia Formations (Fig. 3).

Ultima Esperanza District, Chile

In the Ultima Esperanza district of Chile, the onset of foreland basin sedimentation is recorded in the Punta Barrosa Formation, which generally consists of packages of interbedded sandstone and mudstone and has an overall estimated thickness of about 1 km (Wilson, 1991; Fildani *et al.*, 2003). Wilson (1991) described the transition from the underlying Zapata Formation to the Punta Barrosa Formation as being marked by the 'abrupt', consistent presence of medium-grained sandstone beds that range from 30 to 100 cm in thickness; however, Fildani & Hessler (2005) suggest that the contact is more subtle and consists of a *ca.* 150-m-thick transition zone within which a precise boundary cannot be placed. The transitional

stratigraphy between the underlying Zapata Formation and the Punta Barrosa (informally called the Zapata–Punta Barrosa transition, nomenclature of Fildani & Hessler, 2005) has a reported radiometric age of 101 ± 1.1 Ma (Fosdick *et al.*, 2011). Detrital zircon ages from multiple sandstone units suggest an overall maximum depositional age of *ca.* 92 Ma for the Punta Barrosa (Fildani *et al.*, 2003). Detrital zircon age determinations are younger than previous interpretations of a late Albian to Cenomanian age based on a sparse ammonite assemblage (Cortés, 1964).

The Punta Barrosa Formation has been interpreted to primarily reflect high- and low-density turbidity currents deposited in an unconfined deep-water depositional setting (lobes) within the axis of a constricted foreland basin trough (Fildani & Hessler, 2005; Romans *et al.*, 2011). Paleocurrent indicators from the Punta Barrosa Formation consistently result in south to southeast palaeoflow suggesting that sediment dispersal was parallel to the axis of the foreland basin (Cortés, 1964; Wilson, 1991; Fildani & Hessler, 2005).

Cordillera Darwin, Chile

South of Ultima Esperanza, Punta Barrosa Formation facies equivalents have been documented as far as the Cordillera Darwin (53–54°S) in Chile (Fig. 1) (McAtamney *et al.*, 2011). These units are referred to as the Latorre (Seno Otway and Peninsula Brunswick) and Upper La Paciencia Formations (Bahia Brooks). Estimated minimum stratigraphic thicknesses range from 600 to 800 m, but may be as thick as 1200 m at Peninsula

Brunswick (McAtamney *et al.*, 2011). These strata generally consist of interbedded fine- to medium-grained sandstone and mudstone with occurrences of coarse-grained sandstone to pebble conglomerate. Similar to the Ultima Esperanza area, coarse-grained strata lie above thick successions of thin-bedded mudstone and mark the initial appearance of continuous, coarse-clastic (medium-grained sandstone to pebble conglomerate) deposition. Consequently, they are also interpreted as the onset of foreland basin sedimentation in this portion of the Magallanes Basin (Mpodozis *et al.*, 2007; McAtamney *et al.*, 2011). Maximum depositional ages determined from detrital zircon age populations are estimated to be as old as 89 Ma, but may be as young as 85 Ma (McAtamney *et al.*, 2011).

Austral Basin, Argentina

Although fluvial and shallow-marine deposits appear as the dominant facies early in the evolution of the northern (Austral) basin sector, the northern extent of deep-water facies was unknown. Deep-marine deposits have been described from outcrops near Lago Argentino as undifferentiated units of the Cerro Toro Formation (Arbe & Hechem, 1984). These outcrops were recognised as early basin fill deposits of Cenomanian–Turonian age and interpreted as low- and high-density turbidites with a southward palaeoflow (Arbe & Hechem, 1984). North of Lago Argentino, age-quivalent strata consist of shallow- to nonmarine deposits of the Lago Viedma (cf. Arbe, 2002) and Mata Amarilla (cf. Varela *et al.*, 2013) Formations (Fig. 3). These formations are underlain by deltaic and fluvial facies of the Albian-aged Piedra Clavada Formation (Poire *et al.*, 2002) near Lago Viedma and north.

METHODS

To better constrain the character and distribution of facies as well as their timing of deposition, this study combines field-based observations and interpretations with U-Pb geochronology of zircon extracted from ash horizons interbedded within these strata. All data were collected from various along-strike locations within the Austral Basin as for north as El Chalten to as far south as the Brazo Sur (Figs 4 and 5). Sedimentologic and stratigraphic data include general observations of lithology, bedding characteristics and architecture as well as palaeocurrent measurements, and photopan interpretations. In addition, this study includes detailed measured stratigraphic sections, which document centimetre-scale variations in grain size and bed thickness as well as the presence and/or absence of sedimentary structures. A total of 321 palaeocurrent measurements were collected; the majority (approximately two-thirds) of the measurements come from sole marks (tool marks, grooves, flute casts, etc.) and the remainders are from ripple cross-laminations.

Eight samples were collected from volcanic ash horizons that are sparsely interbedded within the Punta Barrosa Formation and equivalent strata throughout the study area (Figs 4 and 5). In addition, a detrital zircon sample was collected from the Loma de las Pizarras (LDLP) outcrop near the base of the section (Fig. 5), which constrains the maximum age of deposition and provides important provenance information. U-Pb analyses by laser ablation-inductively coupled plasma mass spectrometry (LA-ICPMS) were conducted and reduced at the Arizona Laserchron Center following methods described in Appendix S1.

STRATIGRAPHY

Outcrop descriptions

Although exposures of the Punta Barrosa Formation and equivalent strata are nearly continuous along the outcrop belt, this study highlights stratigraphic and sedimentological data from four general locations within the Austral Basin. The furthest north is a *ca.* 50 m section exposed along the LDLP ridge within the Parque Nacional los Glaciares near the town of El Chalten, Argentina (Fig. 4). The second location consists of a *ca.* 100-m section located on Estancia Los Hermanos (ELH) near the southern shore of Lago Viedma (Fig. 5). The third is a nearly continuous *ca.* 200 m section that is located along the shoreline on the southern side of the Magallanes Peninsula and is herein referred to as the Magallanes Peninsula (MP) section (Fig. 5). Finally, the fourth and southernmost location in the study area includes a continuous *ca.* 300 m section along the shoreline of the southwest shore of Brazo Sur (Lago Argentino) and will herein be referred to as the Brazo Sur (BS) section (Fig. 5). Additional observations, interpretations and samples come from locations within Zona Centro including exposures near the Rio Guanco (RG) and near the northern shore of Lago Argentino (Fig. 5). Figure 6 shows examples of the outcrop expression of the LDLP, MP and BS sections. The following includes general descriptions and observations from these four exposures, discussed from north to south.

Loma de las Pizarras Section

The LDLP section displays *ca.* 50 m of interbedded sandstone and mudstone that conformably overlies >100 m of mudstone, and gradually transitions upward into more sand-rich units (Figs 6a and 7a). Bed thicknesses range from a few centimetres up to 2 m thick (Fig. 7a). All beds show tabular geometries and consist of grain sizes that range between mudstone and medium-grained sandstone. Amalgamation of sandstone beds is also common within coarser-grained intervals. Many of the beds in this section appear massive (structureless), but otherwise consist of units that are normally graded and commonly contain dewatering structures and mudstone
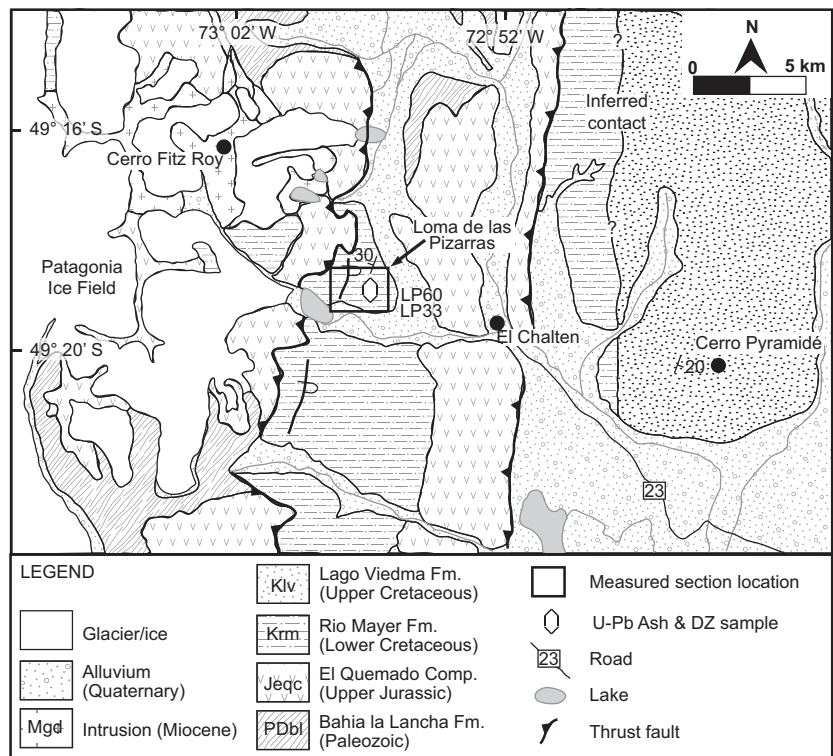
Fig. 4. Geologic map of the northern-most study area surrounding El Chalten, Argentina. Modified from Kosmal & Spikermann (2001). This study area highlights the Loma de las Pizarras (LDLP) outcrop (see Figs 7 and 9) as well as U–Pb ash sample LP60 and U–Pb detrital zircon sample LP33 (Figure 17).

rip-up clasts. There are also rare occurrences of planar laminations and ripple cross-laminations.

Estancia Los Hermanos Section

Outcrops within the Zona Centro region record important variations in depositional context of the Punta Barrosa Formation within the Austral Basin (Fig. 5). The ELH section located near the southern shore of Lago Viedma, exposes an approximately 100-m section that provides an unparalleled view of bedding geometries and lateral facies relationships within the lower Punta Barrosa Formation. The ELH outcrop is comprised of several distinct packages of medium- to thick-bedded sandstone that are encased in mudstone-dominated intervals (Fig. 8). The majority of this outcrop consists of chaotically bedded units that are particularly common in the mudstone-dominated facies. These deformed zones are bounded above and below by continuous horizons, and they are interpreted as mass-transport deposits (MTDs; Shipp *et al.*, 2011). Several of these discrete sandstone packages transition laterally to a more chaotic expression at the southern end. For example, two of the sandstone packages develop into a series of multiple, imbricate thrust faults that are generally verging towards the north (Fig. 8).

Several north-dipping normal faults are present that offset both mudstone- and sandstone-dominated units within the ELH outcrop. These faults likely formed synchronously with deposition and are interpreted as growth faults because: (1) these faults terminate up-section and are overlain by continuous bedding with no apparent offset, (2) these faults have a roughly listric geometry and (3) sandstone packages thicken towards the footwall and

abruptly thin away from the fault (Fig. 8). In addition, one sandstone package shows an apparent on-lapping relationship with the underlying mudstone that may relate to synchronous growth on an adjacent normal fault (Fig. 8).

Magallanes Peninsula Section

The MP section is approximately 180 m of continuous stratigraphy with excellent exposure quality (Figs 6b and 7b). This section consists largely of interbedded mudstone and sandstone (up to medium-grained sandstone) and tabular, laterally extensive (100s of metres) bedding geometries (Fig. 6b). Bed thicknesses range from very thin-bedded (3–5 cm) up to medium bedded (1.5 m) (Fig. 7b). The majority of the beds are normally graded with fine- to medium-grained sandstone at the base and siltstone and/or mudstone at the top. Common structures include planar laminations, ripple cross-laminations, dewatering structures, mudstone rip-up clasts and flame structures. Bioturbation is also common within mudstone intervals. This outcrop also includes an abundance of argillaceous (mud-rich) sandstone beds, which are discussed later in the text. A total of 29 palaeocurrent measurements were collected from the MP section, which includes 11 sole marks and 18 ripple laminations (Fig. 5). Sole marks indicate a general southward palaeoflow, whereas ripple laminations suggest more of an east-south-east palaeocurrent direction.

Brazo Sur Section

The Punta Barrosa Formation at the southern end of Brazo Sur preserves at least 300 m of continuous strati-
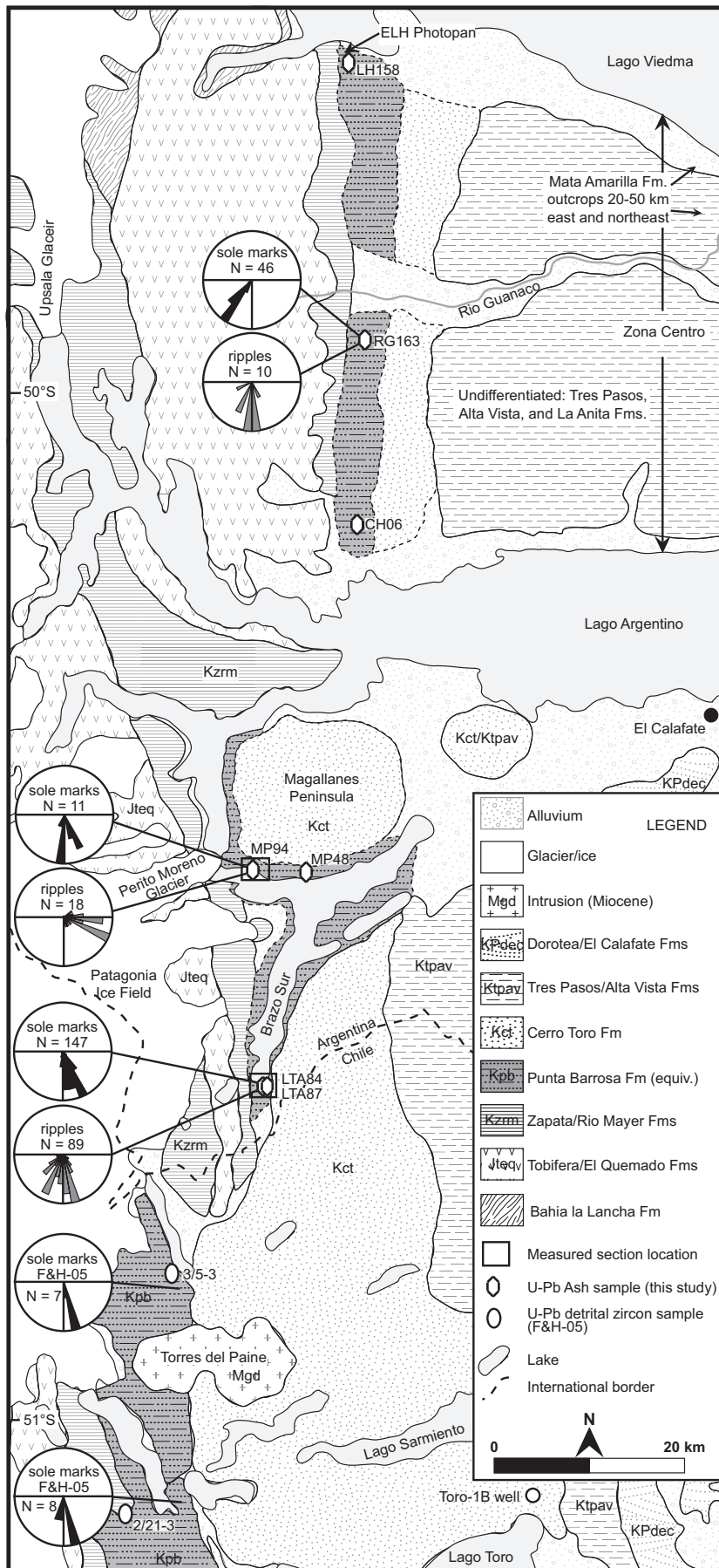
Fig. 5. Geologic map of the northern Ultima Esperanza District of Chile and northwards to Lago Viedma, Argentina. Samples and palaeocurrent data denoted with F&H-05 corresponds to results reported by Fildani & Hessler (2005). Modified from Ghiglione *et al.* (2009).
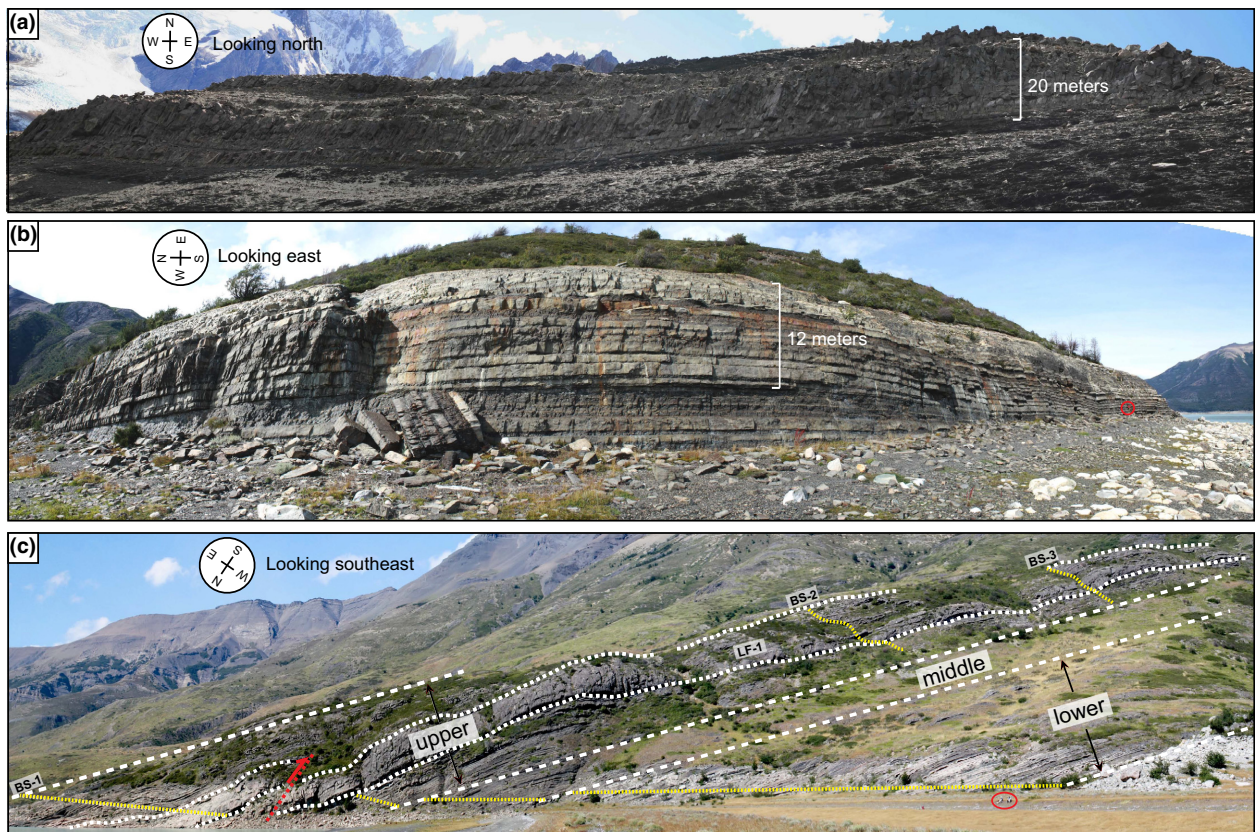
Fig. 6. Photos showing the outcrop character of Punta Barrosa equivalent units in Argentina. (a) Lower section of stratigraphy from Loma de las Pizarras near El Chalten, (b) lower portion of section from the Magallanes Peninsula showing tabular bedding geometries, person circled for scale and (c) photopan showing nearly the entire outcrop at Brazo Sur. Yellow dotted lines denote the approximate routes, where sections were measured (people circled for scale).

graphic section and, to our knowledge, also represents the most complete documented section of the Punta Barrosa Formation facies equivalent rocks. For descriptive purposes, this section is informally divided into lower, middle and upper sections (Fig. 6c). These are not intended to correspond to upper and lower Punta Barrosa divisions that have been described in the Magallanes Basin (Wilson, 1991; Fildani & Hessler, 2005).

The lower section is at least 120 m thick and primarily consists of tabular beds of mudstone and fine- to medium-grained sandstone (Fig. 9). Bed thicknesses are variable, but typically in the range of 20 to 100 cm. Similar to the stratigraphy at MP, the majority of the beds in this section are normally graded with fine- to medium-grained sandstone at the base and siltstone and/or mudstone at the top. Common structures include planar laminations, ripple cross-laminations, dewatering structures, mudstone rip-up clasts and flame structures. This section also contains the majority of argillaceous sandstone beds identified from the entire BS section.

The middle section consists of approximately 70 m of very thin- to thin-bedded mudstone, siltstone and very fine- to fine-grained sandstone. Initially this interval fines upward (increasing mudstone/sandstone ratio) and then gradually shifts back to a slightly upward coarsening trend with increasing proportions of sandstone beds (Fig. 9).

All beds show tabular geometries and rarely exceed thicknesses of 25 cm. Sandstone intervals commonly exhibit planar laminations and ripple cross-laminations, while mudstone intervals are typically massive and bioturbated. This middle section gradually transitions upward into coarser-grained facies of the upper section.

Last, the upper section of the Punta Barrosa Formation at Brazo Sur is represented in the upper 110 m of the stratigraphic section (Fig. 9). Overall, amalgamation is much more common, especially in the lower 30 m of the interval, and bedding geometries are commonly lenticular or uneven (Figs 9 and 10). In this section, bed thicknesses is up to 5 m, and are coarser grained (gravel-sized conglomerate). The coarse-grained, amalgamated interval is well exposed and has a basal surface that can be traced laterally for at least 400 m (Fig. 10). Also, compared with the lower and middle sections, finer-grained facies are more bioturbated, pervasively ripple cross-laminated and often consist of intervals of repetitive thicknesses.

Paleocurrent indicators (ripples, flutes and grooves) are abundant throughout the outcrop. A total of 236 measurements were collected and include 147 sole marks and 89 ripple laminations. Sole marks indicate a consistent south-southeast palaeoflow and ripple laminations show a bit more variation between a southwest to southeast palaeoflow (Fig. 5). Also, sandstone injectites (clastic dikes) are
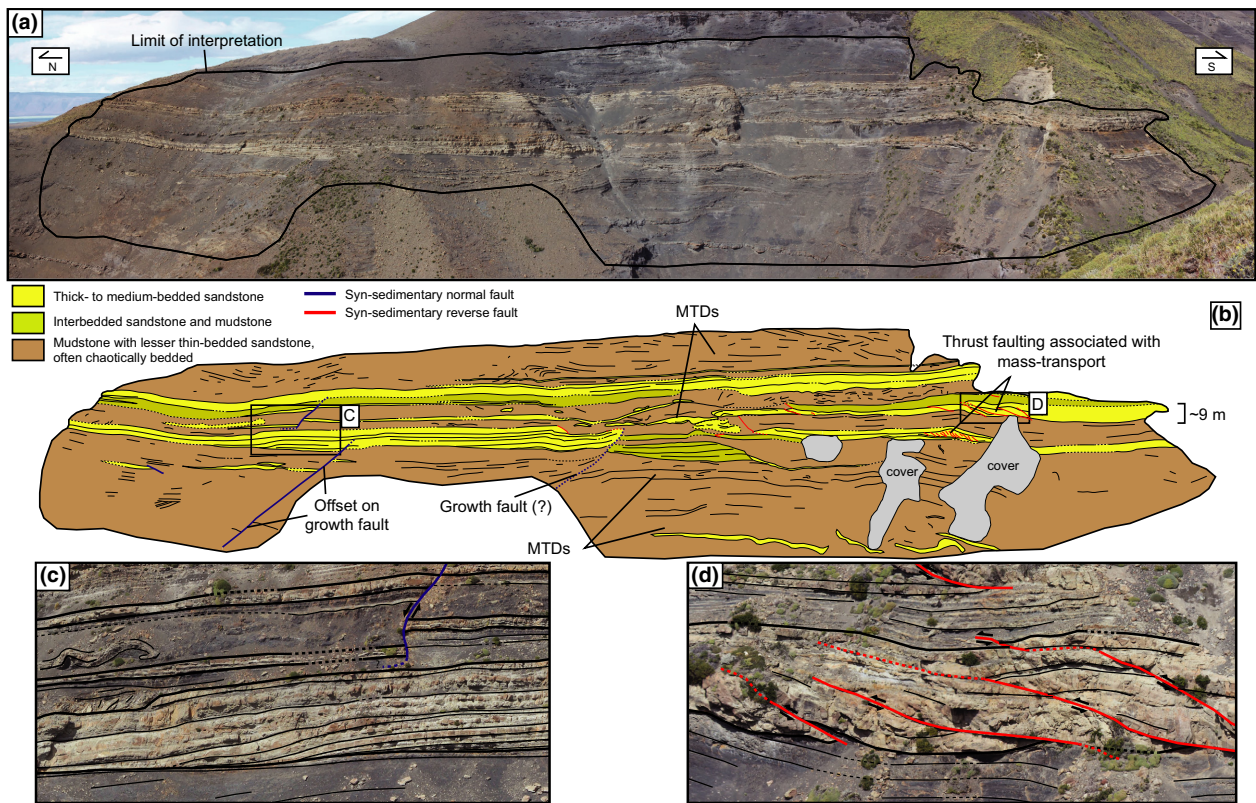
Fig. 7. Measured stratigraphic sections from Loma de las Pizarras (a) and the Magallanes Peninsula (b).

Fig. 8. Photopan (a) and interpretation (b) of the outcrop near Estancia Los Hermanos (ELH) including the presence of growth faults, on-lapping sandstone packages (c), mass transport deposits (MTDs) and imbricated sandstone beds (d).

common throughout the entire BS section, but are especially abundant in the upper 50 m of the upper interval.

Lithofacies

Measured stratigraphic sections document bed scale (centimetre to decimetre) features that include grain size, bed thickness, sedimentary structures and bedding geometries. These sections were then divided into lithofacies which correspond to groups of beds with similar characteristics, most notably grain size and bed thickness in this case (Fig. 11). The usage of lithofacies in this context is most similar to schemes that use third-order architectural elements to describe deep-water stratigraphic architecture (e.g. Ghosh & Lowe, 1993; Lowe & Ghosh, 2004; Anderson *et al.*, 2006; Hubbard *et al.*, 2008). The following descriptions of lithofacies are the result of combined observations and interpretations from LDLP, MP and BS outcrop locations. Detailed stratigraphic sections from each location and the interpreted distribution of lithofacies are shown in Figs 7, 9 and 10.

Measured stratigraphy from the Argentine sector of the basin can be subdivided into five basic lithofacies (Fig. 11, Table 1): (1) thick-bedded sandstone and conglomerate, (2) thick-bedded sandstone and minor mudstone, (3) medium-bedded sandstone and mudstone, (4) thin-bedded sandstone and mudstone and (5) thin-bedded siltstone and mudstone. Beds from all lithofacies are interpreted as individual sedimentation units resulting

from sediment gravity flow deposits, including turbidity currents, debris flows and transitional (or hybrid) flows (cf. Haughton *et al.*, 2009). Internal divisions of low- and high-density sediment gravity flow deposits correspond to those assigned by Bouma (1962) and Lowe (1982), respectively.

LF-1: Thick-bedded sandstone and conglomerate

Description. Deposits of thick-bedded, medium-grained sandstone to gravel-sized, clast-supported conglomerate represent the coarsest facies observed in the Punta Barrosa Formation and are only present within one interval at the BS location (Figs 9 and 10). Individual beds are up to 5 m thick, but commonly range from 0.5 to 1.5 m thick. Bedding geometries are often irregular and lenticular as basal scour and amalgamation are common (Fig. 12a). Sedimentation units are typically normally graded and occasionally exhibit planar laminations (T_b), but are otherwise structureless (S_3/T_a). Additional features include dish and pillar dewatering structures as well as flute casts, grooves and tool marks. Although rarely preserved in these units, mudstone and siltstone intervals can be up to 5 to 10 cm thick and occasionally contain sand-filled burrows (*Thalassinoides*).

Interpretation. Massive (structureless) sandstone intervals that are abundant in the lower portions of beds represent S_3 divisions of high-density turbidites (Lowe, 1982).
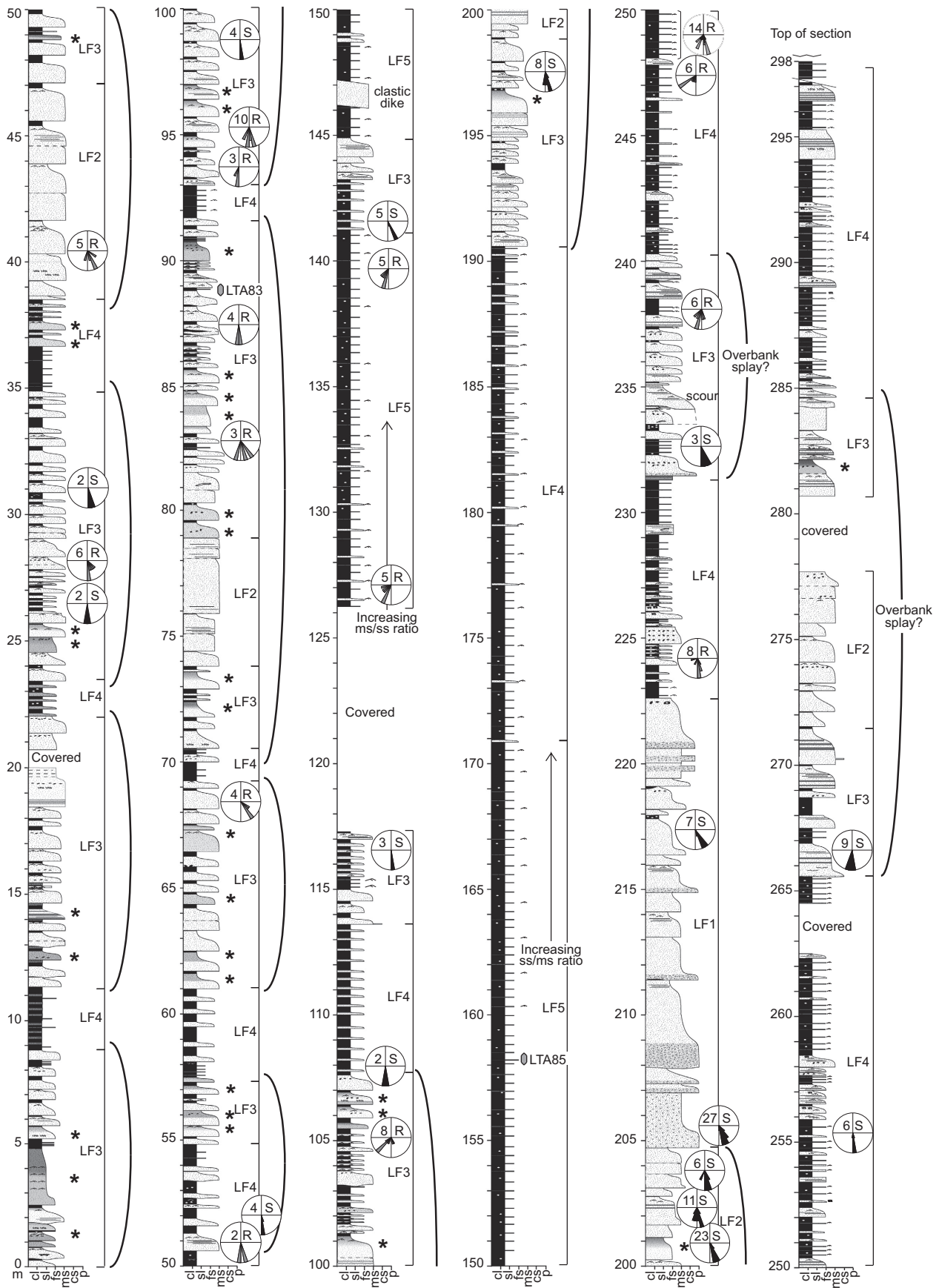
Fig. 9. Measured stratigraphic section from Brazo Sur. See Fig. 6 for photopan of the outcrop. See Fig. 7 for legend.
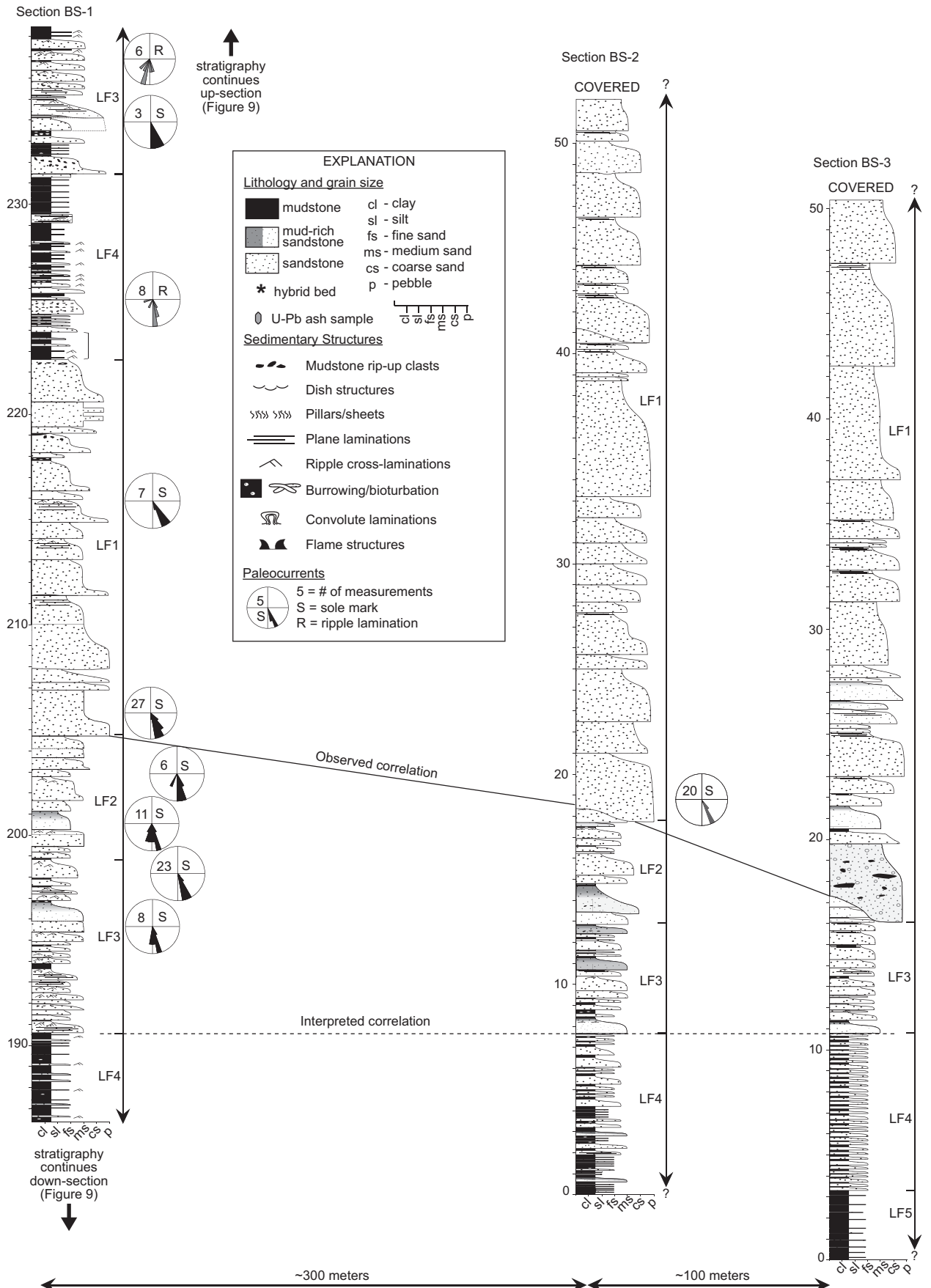
Fig. 10. Lateral correlation of LF-1 units from sections measured at Brazo Sur. Note the lateral thickness variations (*ca.* 18–34 m) in LF–1. See Fig. 5 for section locations on outcrop.
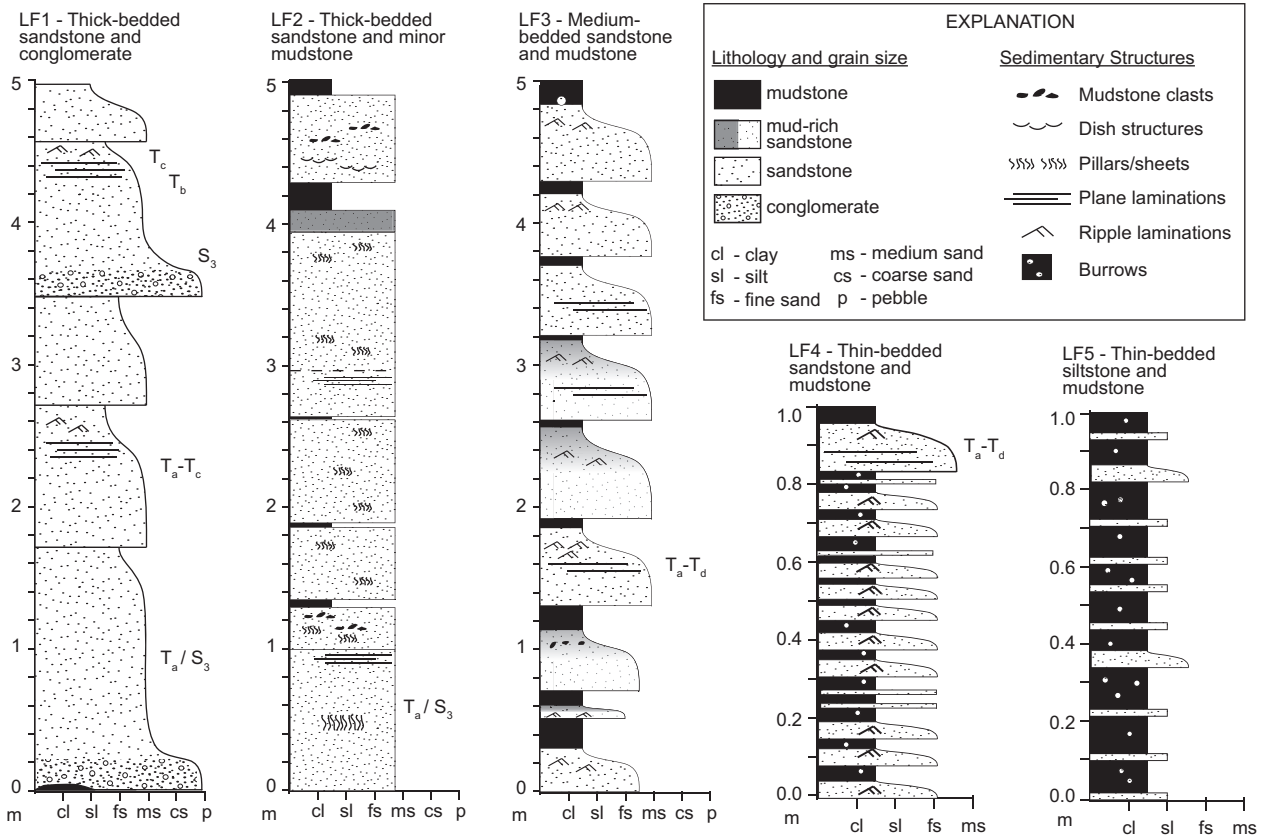
Fig. 11. Examples of the five lithofacies identified in outcrop. See text for descriptions and interpretations.

Water escape structures reflect density instabilities of trapped fluids due to rapid deposition of waning flows. Planar laminated beds are interpreted as high velocity T_b divisions of low-density turbidity currents (Bouma, 1962). Lenticular bedding geometries, the abundance of amalgamated beds, basal scour and the presence of conglomerate suggest that these deposits represent laterally confined flows, which we interpret as indicating a channelised depositional setting.

At Brazo Sur, two additional stratigraphic sections (BS-2 and BS-3) were measured through this interval to compare laterally equivalent facies (Fig. 10). Although the lack of continuous lateral exposure makes it difficult to correlate these sections, at least one surface along the base of LF-1 can be traced along the outcrop. Locally, this surface commonly shows down-stepping (towards the west-southwest) into underlying beds (Fig. 12b). Furthermore, in sections BS-2 and BS-3, lithofacies 1 is nearly double the thickness (*ca.* 34 m) compared with that of BS-1 (18 m) (Fig. 10). We interpret the down-stepping and lateral thickness changes as additional evidence for the presence of channelisation within a confined system.

LF-2: Thick-bedded sandstone and minor mudstone

Description. Thick beds of fine- to coarse-grained sandstone with minor mudstone are present within all three measured sections. Bed thicknesses range from 25 to 200 cm, but are typically 40 to 120 cm thick (Fig. 11). Bedding geometries are mostly even (tabular) and occasionally irregular (undulose) at the base. Amalgamation of sandstone units is common, but basal scour and erosion are rare. Sandstone beds are most commonly massive (S_3/T_a), normally graded and contain dish and/or pillar structures. Planar laminations (T_b) and mudstone rip-up clasts are common while ripple cross-laminations (T_c) are rare. Where preserved, mudstone portions of sedimentation units are less than 10 cm thick, appear massive and are occasionally bioturbated.

Interpretation. Lithofacies 2 is interpreted to reflect rapid deposition of mostly high-density turbidity currents. Amalgamation of sandstone beds, mudstone rip-up clasts and infrequent preservation of mudstone horizons suggest that flows were energetic enough to remove finer-grained caps of previous flows, but unable to maintain suspension of sand. Conditions of collapsing flows (rapid deposition) are supported by the pervasive abundance of dewatering structures (dishes and pillars). An unconfined to weakly confined depositional setting is interpreted as a result of beds being laterally continuous and showing mostly even thicknesses at the extent of the outcrop. We interpret the rapid deceleration and collapse of these flows to broadly reflect a channel-to-lobe transitional setting (e.g. Howell & Normark, 1982; Mutti & Normark, 1987; Wynn *et al.*, 2002; Van der Merwe *et al.*, 2014).

Table 1. Descriptions and characteristics of lithofacies

| Lithofacies	Grain size	Bed thickness	Bed Geometry	Sedimentary structures	Secondary and notable features	Depsotional process
LF1 Thick-bedded sandstone and conglomerate	Medium-grained sandstone to conglomerate (clasts up to 2 cm dia.) rare mudstone	Generally 50–150 cm, range from 30–200 cm	Irregular and lenticular	Massive (T_a/S_3) divisions, normal grading, occasional planar laminations (T_b)	Basal scour, amalgamation, sole marks (flutes/tools), dish and pillar dewatering structures	Rapid deposition of mostly high–density turbidity currents in a moderate to weakly confined setting
LF2 Thick-bedded sandstone and minor mudstone	Fine- to coarse-grained sandstone and occasional mudstone	Generally 40–120 cm, range from 25–200 cm	Tabular and even occasionally irregular	Massive (T_a/S_3) divisions, normal grading, occasional planar laminations (T_b), rare ripple cross-laminations (T_c)	Amalgamation, dish and pillar dewatering structures, mud rip-up clasts and occasional sole marks	Rapid deposition of low– and high–density turbidity currents in a weakly confined to unconfined setting
LF3 Medium-bedded sandstone and mudstone	Mudstone, siltstone and fine- to medium–grained sandstone	Generally 30–80 cm, range from 20–120 cm	Mostly tabular, occasionally irregular to lenticular	Massive (T_a/S_3) divisions, normal grading, planar laminations (T_b) and ripple cross-laminations (T_c) are common, mudstone units are typically massive, occasionally laminated	Dish and pillar dewatering structures, mud rip–up clasts, occasional sole marks, bioturbated sandstone and mudstone units, sandstone beds w/ variations in mud content at discrete boundaries (hybrid beds)	Deposition by low–density turbidity currents, debris flows and/or hyrdid flows in an unconfined setting
LF4 Thin-bedded sandstone and mudstone	Mudstone, siltstone and fine-grained sandstone, rare medium–grained sandstone	Generally 5–20 cm, range from 3–30 cm	Tabular and even	Normal grading, planar laminations (T_b) and ripple cross-laminations (T_c) are common, occasional massive (T_a) sandstone divisions, mudstone units are typically massive, occasionally laminated	Mudstone units commonly bioturbated, occurences of mud ripup clasts and convolute laminations	Deposition by low–density turbidity currents in an unconfined setting in an offaxis or distal position to the locus of deposition
LF5 Thin-bedded siltstone and mudstone	Mostly mudstone and siltstone with occasional fine-grained sandstone	Generally 5–15 cm, range from 2–20 cm	Tabular and even	Normal grading, occasional ripple cross-laminations (T_c) and rare planar laminations (T_b), mudstone and siltstone units are typically massive, occasionally laminated	Mudstone units are pervasively bioturbated	Deposition by low–density turbidity currents and hemipelagic suspension settling in an unconfined setting in an off-axis or distal position to the locus of deposition
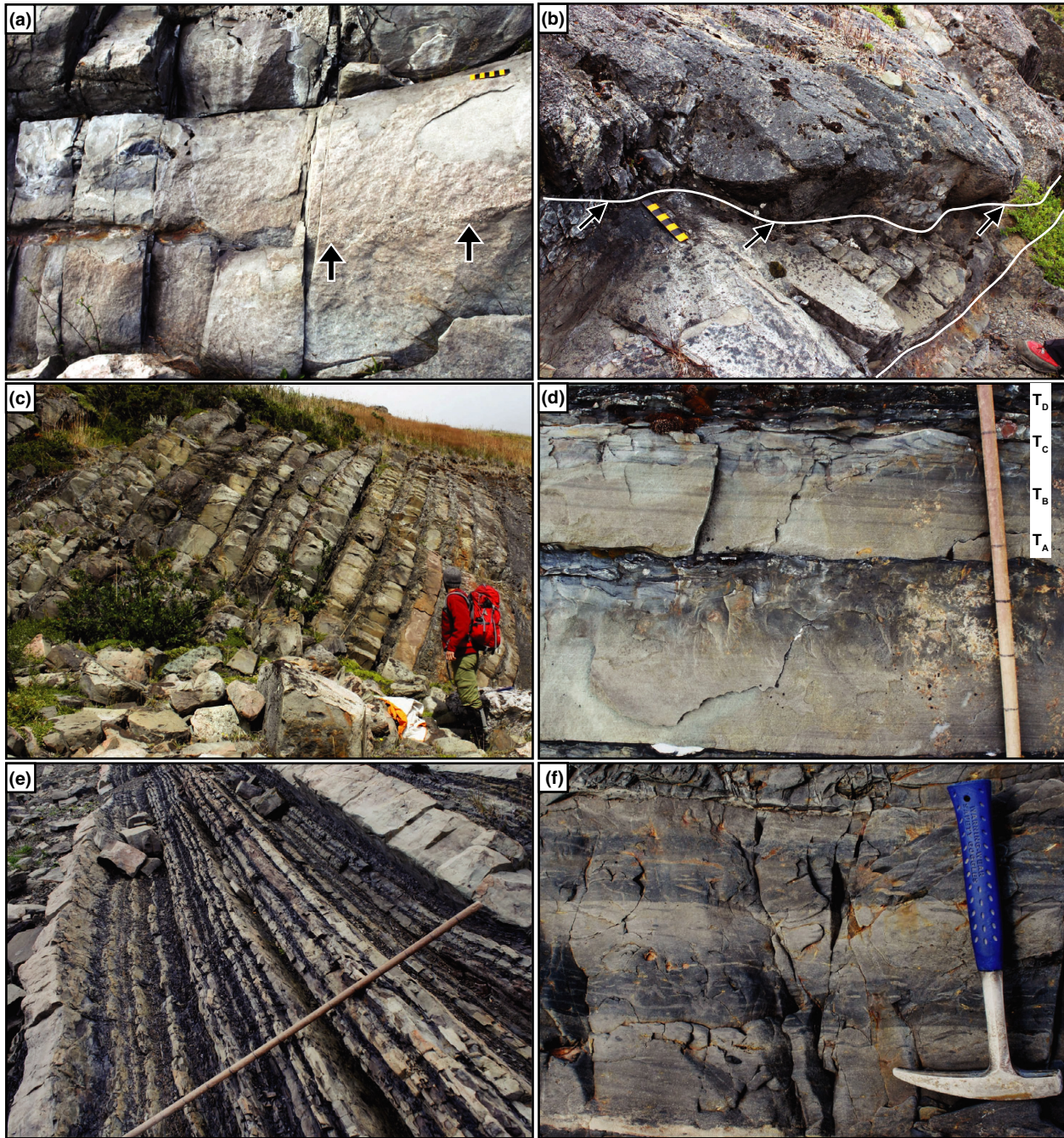
Fig. 12. Examples of bedding style and sedimentological character. (a) Lenticular beds showing basal scour and amalgamation that is common in LF1. Scale is 16 cm. (b) Localised scouring (down-stepping towards the southwest) of LF1 in the BS-2 section. Scale is 16 cm. (c) Example of tabular units of interbedded sandstone and mudstone (LF3). (d) Upper bed shows preservation of T_a–T_d Bouma divisions. Scale in 10 cm increments. (e) Repeated beds of thin, low-density turbidites characteristic of LF4. Scale in 10 cm increments. (f) Bioturbated siltstone and mudstone beds (LF5).

LF-3: Medium-bedded sandstone and mudstone

Description. Lithofacies 3 consists of medium-bedded, fine- to medium-grained sandstone and mudstone and represents the overall most abundant lithofacies. Individual beds are generally 30 to 80 cm thick, but range from 20 to 120 cm thick, and usually consist of tabular geometries with rare occurrences of uneven thicknesses or lenticularity (Figs 11 and 12c). Tabular beds can be traced laterally for the entire extent of the outcrop, up to 250 m in some cases (Fig. 6b). Nearly all sedimentation units are normally graded and have a massive sandstone interval (T_a) at the base and a mudstone/siltstone upper interval (T_d). Sandstone beds are rarely amalgamated. Current-structured intervals such as planar laminations (T_b) and ripple cross-laminations (T_c) are also common (Fig. 12d). Other common structures/features include dish and pillar structures, mudstone-rip up clasts and occasional sole

marks (flutes and grooves) at the base of beds. The mud–stone portions (T_d) of beds are typically silty and massive, and rarely exhibit horizons of strictly claystone (T_e). Trace fossils are common within this lithofacies and most commonly include *Thalassinoides* and *Ophiomorpha,* as well as fewer occurrences of *Spyrophyton*, *Scolicia* and *Skolithos*.

Another important characteristic of this lithofacies is the presence of argillaceous (mud-rich) sandstone beds with varying concentrations of mud that occur at discrete intervals within a bed (Fig. 13). These beds typically contain cleaner (mud-poor) sandstone intervals at the base that abruptly transition upward into more mud-rich sandstone divisions with dewatering pillars and mudstone rip-up clasts. It is also common for argillaceous units to exhibit one or more current-structured intervals (e.g. planar laminations and/or ripple cross-laminations).

Interpretation. Lithofacies 3 is interpreted to reflect the deposition from a range of sediment gravity flow types including low-density turbidity currents, transitional flows and debris flows. Clean (mud-poor) sandstone beds commonly exhibit one or more divisions ($T_{a–d}$) of low-density turbidites (Bouma, 1962). Argillaceous sandstone beds with discrete intervals of varying mud concentration are interpreted as transitional flow deposits or 'hybrid event beds' (cf. Haughton *et al.*, 2009) or 'slurry beds' (Lowe & Guy, 2000). Instances where sandstone beds appear mud-rich throughout and do not show transitions in mud content (except for mudstone caps) are interpreted as debris flow deposits. In all cases, the abundance of tabular bedding geometries and preservation of mudstone divisions indicates that these flows were generally nonerosive and unconfined. Similar facies characteristics have been described in the Magallanes Basin by previous workers and interpreted as lobes (i.e. sheets or splays)
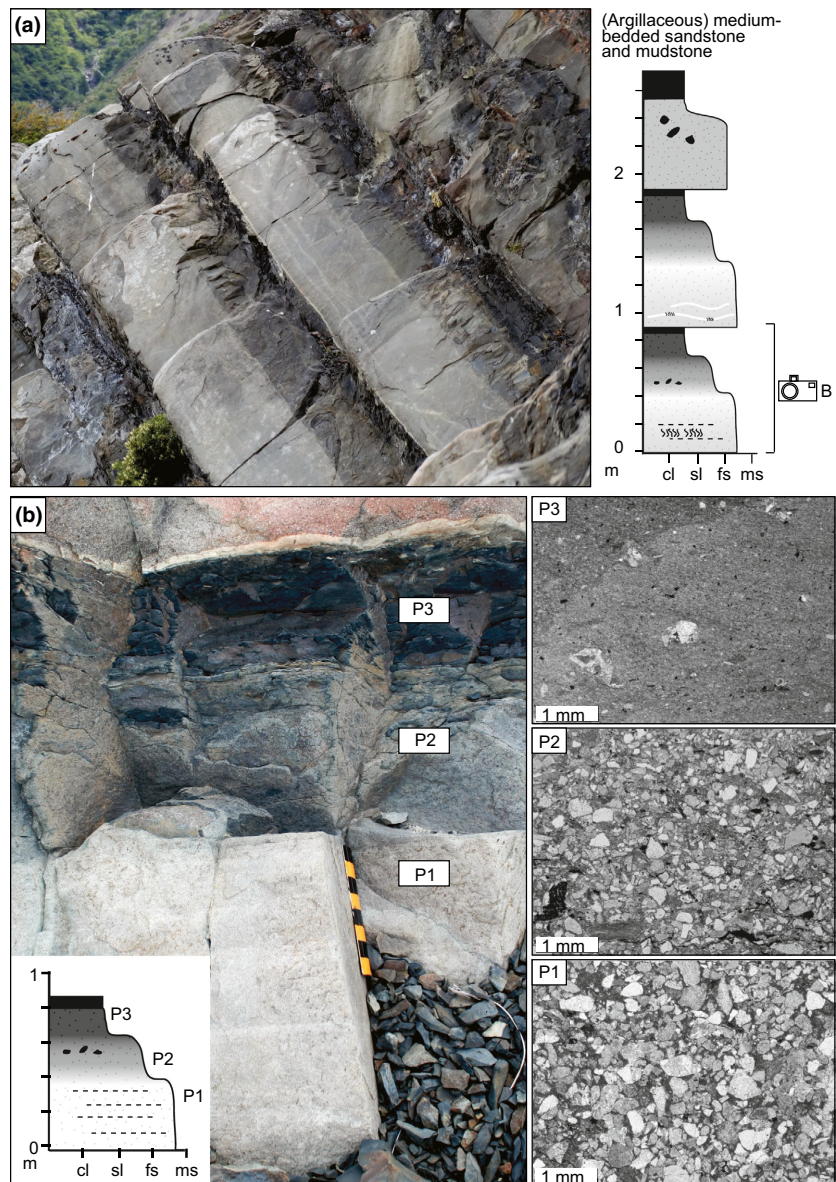
Fig. 13. Characteristics of hybrid beds from the Magallanes Peninsula. (a) Representative bed-scale characteristics of multiple hybrid beds, which are commonly associated with LF-3. See section adjacent to photo for scale. (b) Example of within-bed features showing abrupt changes in colour and inferred detrital mud content. Locations of thin section photomicrographs identified as P1, P2 and P3. Although sand-sized grains are present throughout, the apparent mud concentration increases upward in the bed.

along a fan setting (Wilson, 1991; Fildani *et al.*, 2007; Romans *et al.*, 2011).

LF-4: Thin-bedded sandstone and mudstone

Description. Lithofacies 4 consists of thin beds of mudstone, fine-grained sandstone and rare medium-grained sandstone. Individual beds are most commonly 5 to 20 cm thick, but can be up to 40 cm thick (Figs 11 and 12e). Beds are tabular and typically exhibit even thicknesses at the scale of the outcrop. Massive basal divisions, planar laminations and ripple cross-laminations are all common in sandstone units. In many instances, near-complete and continuous low-density turbidite divisions ($T_{a–d}$) are preserved (Bouma, 1962). Mudstone units are usually massive and contain burrows. In addition to bed thickness and grain size, these units are most distinguishable from lithofacies 3 and 5 in that they are abundant with current structures (planar laminations and ripple cross-laminations) and are typically 40 to 60 per cent mudstone.

Interpretation. Thin-bedded sandstone and mudstone facies are interpreted as deposits of low-density turbidity currents under waning flow conditions in a relatively distal or off-axis depositional setting (e.g. outer fan, crevasse splay or levee-overbank). The general lack of any scour features, the abundance of current structures (e.g. T_b and T_c divisions), and the presence of tabular, laterally extensive bedding geometries are interpreted to reflect relatively low-energy flows that were unconfined. In some instances, LF-4 likely corresponds to off-axis deposition such as levee-overbank settings; whereas in other cases these facies simply reflect the distal run-out of flows. The discrepancy between these two interpretations is discussed below in more detail.

LF-5: Thin-bedded siltstone and mudstone

Description. Thinly interbedded mudstone facies are primarily mudstone and siltstone, but occasionally include grain sizes up to fine-grained sandstone. Beds are commonly 2 to 15 cm thick and have even, tabular geometries. Sedimentation units are normally graded where they contain enough grain size variation and are otherwise massive. This lithofacies differs from LF-4 in that, overall, it is finer grained (only occasional beds of very fine- to fine-grained sandstone) and consists of thinner beds that rarely exceed 20 cm (Fig. 12f). Bioturbation is abundant as nearly all of the mudstone and siltstone units within this lithofacies contain trace fossils, which commonly include *Scolicia*, *Cosmorhaphe* and *Chondrites*.

Interpretation. Similar to Lithofacies 4, we interpret thin-bedded mudstone and occasional fine-grained sandstone to reflect deposition of low-density turbidity currents in a relatively distal or off-axis depositional setting such as a lower fan, basin plain, or along a slope. The majority of

these units are interpreted to result from sediment fall-out from suspension, as they are typically massive or normally graded. Thick (>5 m) intervals of LF-5 are present at least once in all three sections and likely represent a relatively quiescent time and/or position in the depositional setting of this system.

Interpretation of depositional environments

Deep-marine fan system

We interpret the LDLP, BS and MP outcrops to represent deposition along a deep-marine fan system. This is consistent with previous workers' interpretations of facies equivalent units from the Magallanes basin sector in Chile (Wilson, 1991; Fildani & Hessler, 2005; McAtamney *et al.*, 2011). Bathyal (1000–2000 m) water depths have been determined from biostratigraphic assemblages in the Magallanes Basin (Natland *et al.*, 1974). In addition, the assemblage of trace fossils observed throughout the study area is consistent with those that are common to the *Nereites* ichnofacies (MacEachern *et al.*, 2010). For the purposes of this study, a submarine fan 'system' includes both confined and unconfined elements, which from distal to proximal consist of: basin plain, lower fan, mid fan and upper fan (Ricci Lucchi, 1975; Normark, 1978) (Fig. 14a). Furthermore, similar to other deep-water fan models, this synthesis also includes the interpretation of lobes as smaller scale features that are typically associated with the middle to lower fan region (Fig. 14a) (Ricci Lucchi, 1975; Mutti, 1977; Walker, 1978; Howell & Normark, 1982). Lobe definitions and characteristics are discussed later.

Thin-bedded, fine-grained units of LF-4 and LF-5 are interpreted as distal or off-axis (from any major sediment fairway) deposits in a lower fan to basin plain setting (e.g. Mutti & Ricci Luchi, 1975; Mutti *et al.*, 1978; Howell & Normark, 1982). Overall, LF-3 is the most abundant and we interpret these facies to represent lobes in a mid to lower fan depositional setting. Thicker bedded, and more amalgamated units of LF-2 correspond more closely to mid to upper fan regions where flows are losing confinement and rapidly collapsing. The coarse-grained units of LF-1 are present only in the upper part of the section at Brazo Sur and we interpret these facies to represent confined deposits in the upper fan region, or at least in the vicinity of the channel-lobe transition zone (Mutti and Ricci Lucchi, 1975; Mutti *et al.*, 1978; Howell & Normark, 1982; Mutti & Normark, 1987; Wynn *et al.*, 2002; Van der Merwe *et al.*, 2014).

An important exception to the aforementioned association of LF-4 occurs in the interval that is stratigraphically above the section of LF-1 at Brazo Sur (Figs 9 and 10). Here, the LF-4 interval is laterally equivalent to coarse-grained, amalgamated units of LF-1 (Fig. 10), which suggests that they more likely represent overbank or levee deposits rather than a distal fan setting (Fig. 14b). Thus, the presence of repetitiously thin-bedded, low-density
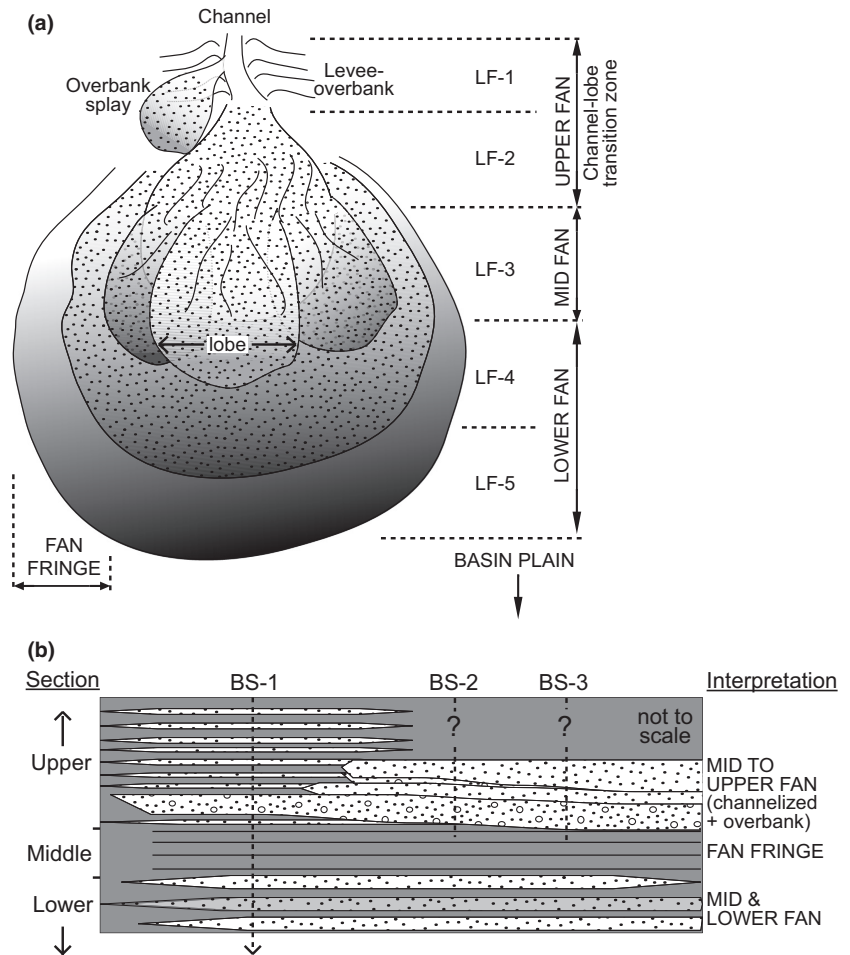
Fig. 14. (a) Depositional setting diagram and nomenclature for submarine fan systems. Modified from Howell & Normark (1982) and references within. (b) Schematic cross-sectional interpretations of the Brazo Sur sections showing the overall progradational architecture from mid-lower fan to upper fan.

turbidites in LF-4 that are laterally equivalent to high-density turbidites of LF-1 reflects processes of flow-stripping whereby flows can overspill confining margins and portions still within the channel rapidly decelerate and collapse due to loss of sediment load and/or loss of confinement (Piper & Normark, 1983). Given this transition in depositional setting, the sandstone intervals of LF-2 and LF-3 that are present above the LF-1 interval at Brazo Sur more likely represent overbank (crevasse) splays rather than mid- to upper fan lobe associations. These interpretations imply that, at least at Brazo Sur, the Punta Barrosa Formation represents an overall progradational system (Fig. 14b). Although previous workers have noted the presence of lobes (or sheets) for the Punta Barrosa Formation in the Magallanes Basin (Fildani & Hessler, 2005; Romans *et al.*, 2011), this interpretation marks the first time that channel and/or levee overbank environments have been suggested for the Punta Barrosa Formation.

Furthermore, LF-3, 4 and 5 constitute the vast majority of Punta Barrosa equivalent outcrops and each of these facies are characterised by tabular beds with mudstone intervals (Bouma T_d and T_e intervals). We interpret this as an indication that once flows reached a fan setting, they were able to sufficiently expand laterally and deposit mud from suspension set-

tling. Consequently, these flows were probably not confined by basin margins or local sea floor topography, except those associated with more amalgamated lithofacies (LF-1 and LF-2).

Slope

The stratigraphy exposed at ELH is interpreted to represent deposition within a deep-water slope setting. This interpretation is based primarily on the evidence for growth faulting as well as the abundance of MTDs that are common in slope settings (Posamentier & Martinsen, 2011). Interestingly, the north-dipping growth faults appear to be antithetic with respect to the overall basin configuration based on documentation of dominantly south-directed palaeoflow throughout the basin (Wilson, 1991; Fildani & Hessler, 2005; this study) and regional palaeogeographic reconstructions (e.g. Romans *et al.*, 2011). Syn-depositional extensional forces along slope settings commonly result in synthetic and antithetic growth faulting (Galloway, 1998; Armentrout *et al.*, 2000; Imber *et al.*, 2003; Shultz and Hubbard, 2005). In addition, observations of the Punta Barrosa Formation at ELH are similar to descriptions of the younger Tres Pasos slope system along El Chingue Bluff in the Magallanes basin (Schultz *et al.*, 2005).

U-PB ZIRCON GEOCHRONOLOGY – SAMPLES AND RESULTS

This study reports new U-Pb geochronology data from eight ash horizons from throughout the Austral Basin and one detrital zircon sample from a sandstone bed at the base of the LDLP section. A summary of sample locations and interpreted ages is available in Table 2. Age data from each sample is shown in Fig. 15 and analytical isotopic data are available in Appendix S2. Results from samples LH158, RG163, LTA87 and MP94 yield MSWD values that are less than the lower bounds of 95% confidence, which suggests that uncertainties in the ages are over–estimated (Mahon, 1996). In part, this may be due low U concentrations in several of the analyses. Nevertheless, all U-Pb ages within each sample's calculated age overlap within 2-sigma error. Uncertainties for each sample age discussed in the text and shown in Table 2 and Fig. 15 are expressed at 95% confidence (*ca.* 2σ).

Sample LP60 was collected from an ash horizon interbedded with mudstone in the northernmost study area approximately 20 m below the base of the LDLP measured section. It yields an interpreted age of 115.1 ± 1.5 Ma (2σ), which is consistent with previous biostratigraphic age constraints that suggest an Aptian–Albian age for this unit (Kosmal & Spikermann, 2001).

Samples LH158, RG163 and CH06 were all collected from thin (2–4 cm) ash horizons in the 'Zona Centro' region, between Lago Viedma and Lago Argentino. Sample LH158 was collected from near the base of the ELH section (Fig. 12) and yields an interpreted age of 100.3 ± 2.7 Ma. RG163 was collected just below the base of a relatively short (*ca.* 20 m) section of sandstone and mudstone, which is internally coherent and it has an interpreted age of 92.3 ± 1.7 Ma. Sample CH06 was collected from Cerro Horqueta near the northern shore of Lago Argentino and yields an interpreted age of 96.5 ± 1.4 Ma.

Two ash samples (MP48 and MP94) were collected from the Magallanes Peninsula and yield interpreted ages of 96.8 ± 1.6 and 95.6 ± 1.5 Ma respectively. Sample MP48 was collected from a roadcut exposure of interbedded sandstone and mudstone. Sample MP94 was collected within the context of the measured section from the Magallanes Peninsula (Fig. 7b).

Finally, samples LTA84 and LTA87 were both collected from ash beds in the context of the measured stratigraphy at the southern end of Brazo Sur (Fig. 9). Sample LTA84 comes from lower in the section and yields an interpreted age of 98.1 ± 1.3 Ma. Sample LTA87 was collected near the middle of the section and yields an interpreted age 97.5 ± 2.1 Ma.

Results of U–Pb detrital zircon ages (*n* = 96) from sample LP33 are shown as a histogram plot and probability density functions in Fig. 15b. Analytical isotopic data are available in Appendix S2. Age populations reveal one primary peak at ca. 110 Ma, and additional, subordinate peaks at 130, 143, 270 and 520 Ma. Given the continuous range of ages between 105 and 135 Ma, a maximum depositional age (MDA) was interpreted by calculating a weighted mean average of the youngest peak age population, which in this case includes 39 ages between *ca.* 105 to 120 Ma. This yields an interpreted MDA of 110.2 ± 1.3 Ma. When accounting for 95% confidence (*ca.* 2σ) limits on the uncertainties the MDA interpreted for sample LP33 is slightly younger (*ca.* 2–5 My) than the interpreted depositional age of sample LP60. In part, this may be a result of the fact that LP60 was collected *ca.* 20 m lower in the section.

DISCUSSION

Lobe dimensions and basin geometry

Given the interpretation that one or more deep-water fan systems represent the early fill of the MAB, we can attempt to learn more about the scale of these systems and the overall basin geometry based on what is known from other fan-lobe complexes. Thrust faulting and folding limit the lateral continuity of outcrops in the study area, however, sections representing submarine lobe facies are well exposed and show vertically stacked packages of beds, which can be interpreted and subdivided into an architectural framework (Fig. 16). Prelat *et al.* (2010) compiled morphological data from six different lobe systems to compare intrinsic and extrinsic relationships of lobe dimensions. They proposed that two general groups characterise the dimensions of lobe deposits: confined and unconfined. Confinement, in this case, refers to basins with steeper gradients perpendicular (or oblique) to flow directions than those parallel, which includes irregular sea–floor topography (Prelat *et al.*, 2010).

Prélat *et al.* (2009) proposed a hierarchical scheme for submarine lobes from the Karoo Basin that emphasises thickness, lithofacies and grain sizes of composite stratal units. For comparative purposes, this study uses a similar scheme in that we define the most basic architectural unit at the bed scale, which corresponds to individual depositional events (e.g. sedimentation units). Also, we define a

Table 2. Locations and U–Pb ages of zircon samples.

Sample ID	Lat (°S)	Lon. (°W)	Interpreted age (Ma)	2σ Error
Ash samples				
LP60	49°19.234	72°57.544	115.1	1.5
LH158	49°40.709	72°49.929	100.3	2.7
RG163	49°58.205	72°48.535	92.3	1.7
CH06	50°09.753	72°48.852	96.5	1.4
MP48	50°29.122	72°57.577	96.8	1.6
MP94	50°28.993	72°58.819	95.6	1.5
LTA84	50°41.602	72° 58.864	98.1	1.3
LTA87	50°41.633	72° 58.705	97.5	2.1
Detrital sample: (location and max. depo. age)				
LP33	49°19.150	72°57.677	110.2	1.3

(a)

(b)
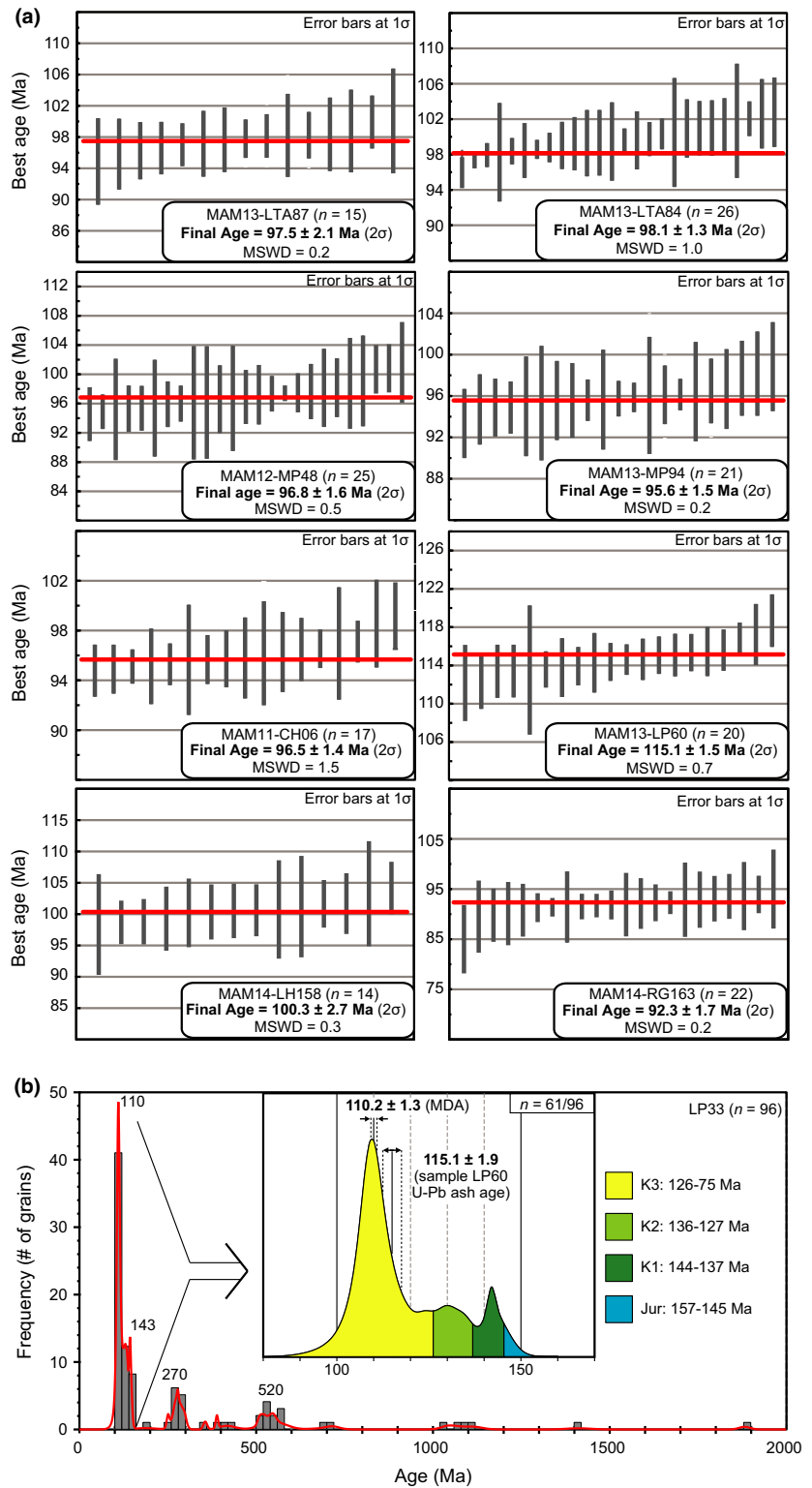
Fig. 15. U-Pb geochronology results. (a) Zircon U-Pb ages of eight ash samples collected from the Austral basin sector. See Figs 4 and 5 for sample locations. (b) Detrital zircon age spectra and relative probably plot of sample LP33 from the LDLP section (see Figs 4 and 7). See text for analytical discussion of results.

lobe as a set of genetically related beds (typically eight or more) that are bound by 'inter-lobe' intervals (commonly >0.5 m thick) of thin-bedded mudstone and sandstone, which likely correspond to lobe margins. Our nomenclature diverges from that of Prelat *et al.* (2010), because in contrast to lobes of the Karoo Basin, the vast majority of beds that are affiliated with lobe facies in this study have preserved mudstone caps. Thus, the application of the

term 'lobe element' as described by Prelat *et al.* (2010) is probably inappropriate for these rocks and thus not employed. Figure 16 shows an example of how this architectural scheme translates to the outcrop at Brazo Sur. In general, the hierarchy used here is closely matched with lithofacies divisions such that LF-2 and LF-3 correspond to lobes and LF-4 and LF-5 are commonly associated with inter-lobe intervals. The following comparison of

Fig. 16. Example photo and measured section from the lower 50 m of the BS section showing how the outcrop expression corr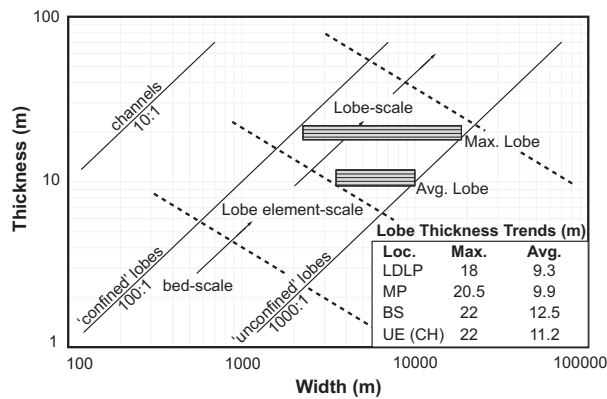esponds to the classification of lobe and inter-lobe (IL) or lobe margin deposits. Red line represents the approximate trace of a small (*ca.* 3 m of offset) localised fault.

the vertical dimensions of lobe facies from our study with their data set allows for a first-order approximation of lobe dimensions and the relative basin geometry during the early history of the MAB.

Figure 17 shows a summary of lobe thicknesses from each of the three sections presented in this study as well as those documented in the Ultima Esperanza District of Chile (Fildani & Hessler, 2005). Maximum lobe thicknesses range from 18 to 22 m and the average from each section/area ranges from 9.3 to 12.5 m (Fig. 17). Plotting this data on fields determined by Prelat *et al.* (2010) suggests that average lobe widths could range from *ca.* 2.5 km (confined system) up to widths of *ca.* 10 km (unconfined system) (Fig. 17). On the basis of the overall prevalence of tabular bedding geometries and preserved mudstone bed-tops, we interpret this to have been a relatively unconfined system and prefer the latter dimensions. In addition, subsurface data from the Toro-1B well drilled in the Ultima Esperanza District of Chile (Fig. 4) revealed that the Punta Barrosa Formation is not present at that location suggesting that it pinches out laterally towards the east within a distance of *ca.* 40 km (Katz, 1963). Depending on the location of the pinch-out, and accounting for *ca.* 30–40 km of thrust-belt shortening (Fosdick *et al.*, 2011) deposits of the Punta Barrosa Formation may have been able to extend laterally for >100 km. The overall geometry of the MAB was likely sufficient for accommodating the spatial capacity of sediment gravity flows into the basin. Thus, these flows were relatively unconfined and probably not affected by the basin margins.

Hybrid event beds

This study highlights the presence of beds that we interpret to have been deposited by flows that included both turbulent and laminar characteristics. Such deposits have been termed hybrid event beds (Haughton *et al.*, 2009) or slurry beds (*sensu*, Lowe & Guy, 2000). In particular, the BS and MP outcrops exhibit excellent exposures of hybrid beds that share similarities with other better-known locations such as the Ross Sandstone Formation in Ireland and the Karoo Basin in South Africa (Haughton *et al.*, 2009; Hodgson, 2009; Talling, 2013). Depositional models for end-member sediment gravity flows and their deposits (e.g. debrites and turbidites) have been available for decades; however, the rheological behaviour of transitional flows and related deposits is still a subject of debate. Recent efforts to constrain the origin and significance of transitional flow processes and the resulting hybrid beds highlight the complexities and challenges associated with these deposits (Lowe & Guy, 2000; Haughton *et al.*, 2003, 2009). In part, these challenges relate to the difficulty in identifying hybrid beds in outcrop because they often require fresh, clean exposures to observe subtle variations in detrital mud content. Similar to turbidity current deposits, there is also a range of vertical profiles that may be expressed in outcrop where only portions of the idealised profiles are preserved (Haughton *et al.*, 2009; Hodgson, 2009).

The interpretation of a depositional setting for rocks of this study was based primarily on bedding geometries, grain size and sedimentary structures and independently

Fig. 17. Plot of lobe dimensions from the Punta Barrosa Formation compared with fields from Prelat *et al.* (2010). Based on thickness trends from this study average lobe widths range from *ca.* 2.5 km (confined systems) to *ca.* 10 km (unconfined systems) and maximum lobe widths may reach up to 20 km.

of the presence and distribution of hybrid beds. Thus, the observations and interpretations may offer insight into the depositional context of transitional flows. A few key observations from this study include: (1) hybrid beds are interbedded with turbidites and debrites; (2) the most abundant vertical facies profile consists of H1, followed by H3, and then capped by an H5 division (Haughton *et al.*, 2009); (3) upward transitions in mud/clay content within beds are typically abrupt and rarely gradational; (4) hybrid beds are most common in the lower portions of the sections at both Brazo Sur and the Magallanes Peninsula, but do occur sporadically throughout each section and (5) hybrid beds are most abundant in facies associated with lobe deposits. An outcrop study from the Karoo Basin found that hybrid beds were most abundant along the fringes of individual lobes and in the more distal (frontal and lateral) positions at the submarine fan scale (Hodgson, 2009). Our interpretations are consistent with these findings as hybrid beds in the Punta Barrosa Formation are most commonly associated with LF-3 and LF-4 (Figs 7 and 9), which correspond to mid to lower (medial to distal) fan deposits (Fig. 14).

Basin-scale variations

There are notable similarities and differences in the lithology, sedimentology and stratigraphic architecture of the Punta Barrosa Formation between the Austral and Ultima Esperanza basin sectors (Figs 2 and 3). Similarities include: (1) Predominant grain sizes consist of mudstone to fine- to medium-grained sandstone; (2) Bedding geometries are mostly tabular at the extent of the outcrop; (3) Interpreted modes of deposition include low- and high-density sediment gravity flows, as well as hybrid deposits and occasional debris flows; (4) Paleoflow was dominantly south directed and (5) the majority of facies suggest deposition along a submarine fan system. Conversely, some important variations are also noted, such as: (1) units in the upper section at Brazo Sur contain gravel

(granule) conglomerates, which is coarser than any of the facies documented to the south in the Ultima Esperanza district; (2) the amalgamation of beds (most notably from the upper section at BS) is more common in the Austral sector; (3) the interpretation of slope facies at ELH was previously unrecognised and 4) the presence of channelised deposits at Brazo Sur. These similarities and differences between units in the Austral sector and UE District of Chile suggest that outcrops in the Austral basin sector represent a more proximal setting, which is largely represented by more amalgamation, thicker beds and coarser grain sizes.

Comparisons with the Punta Barrosa Formation equivalents in the southernmost sector are somewhat limited because the strata from the Cordillera Darwin and Seno Otway have not yet been documented in similar detail. Nevertheless, general descriptions by McAtamney *et al.* (2011) record similar facies and are also interpreted to reflect deposition in a submarine fan setting. Similarly, sandstone beds are described as being in metre- to 10's of metres thick packages, which may be similar in scale to the lobe facies described in this study. However, in contrast to a consistent southward palaeoflow pattern documented in the Ultima Esperanza District as well as this study, palaeocurrent data from the southern basin sector suggests a wider range of sediment dispersal patterns including northeast, east, southeast and southwest (McAtamney *et al.*, 2011).

In summary, submarine fan facies have been interpreted as the depositional setting during the early fill of the MAB from regions as far North as El Chalten (this study) to as far south as the Cordillera Darwin (McAtamney *et al.*, 2011). Yet, there are considerable along-strike variations indicating, at least locally, that the northern Austral sector represents a more source-proximal depositional setting during the early stages of the MAB. These indications are based on the interpretation of slope faces at ELH and the development of a relatively small-channelised system at the BS location.

U-Pb geochronology

Ashes − timing of deposition

New zircon U-Pb ages from ash beds reveal important trends in the early fill of the MAB. Figure 18 plots radiometric age constraints relative to location from throughout the basin, which includes maximum depositional ages interpreted from detrital zircon geochronology by previous workers (Fildani *et al.*, 2003; McAtamney *et al.*, 2011). An overall southward younging trend is shown by the assembly of interpreted depositional ages of units representing the onset of coarse clastic deposition.

Consistent deposition of medium- to thick-bedded sandstone (beds 1–2 m thick) began as early as ca. 115 Ma at the latitude of El Chalten (*ca.* 49°S), which is chronologically associated with the shale-dominated Rio Mayer Formation. Deposition of sand along a deep-water
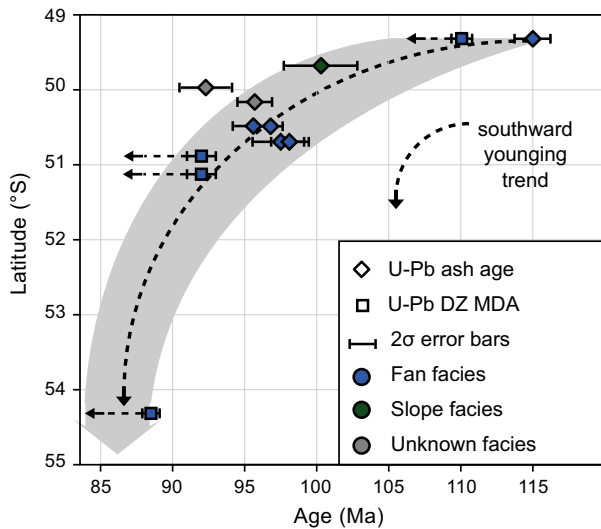
Fig. 18. A plot of interpreted U-Pb ages (Ma) compared with sample locations (latitude) from ash beds and detrital zircon sandstone samples associated with the onset of consistent sandstone deposition in the MAB. Data sources from Fildani *et al.* (2003), McAtamney *et al.* (2011), and this study.

slope is preserved by stratigraphy at ELH and occurs at *ca.* 100 Ma at this latitude. Based on interpretations of the LDLP outcrop, the relative age and depositional setting at ELH suggests a pronounced southward progradation of this deep-water system during Albian time. The other two samples collected from Zona Centro, RG163 and CH06, were collected from outcrops that regionally seem to correspond to the initial consistent appearance of sandstone deposition. Although sample RG163 was collected immediately below the first significant package of sandstone found in the vicinity of the Rio Guanaco, this sample plots slightly off-trend from the other data (Fig. 18). This apparent discrepancy could be due to unaccounted structural complexities within this portion of the fold-thrust belt or could reflect deposition in an off-axis position (mud-dominated) relative to the Punta Barrosa locus of deposition sampled to the north and south. We prefer the latter given that the outcrop at ELH suggests a slope setting for this region as slope settings are commonly characterised by mud deposition (Pickering *et al.*, 1986; Galloway, 1998; Prather *et al.*, 1998).

All four of the U-Pb ash ages from the BS and MP study areas range from 98.1 to 95.6 Ma and are all overlapping when accounting for 2σ uncertainties (Fig. 18). The resolution of these ages precludes from confidently discerning the timing relationships between the BS and MP outcrops. The youngest age interpreted (95.6 Ma) from the southern portion of the Austral sector predates maximum depositional ages of the Punta Barrosa Formation in the Magallanes sector by approximately 3 Myr.

Detrital zircon provenance

U-Pb detrital zircon ages from sample LP33 help constrain the maximum timing of deposition, as well as sedi-

ment sources for these sandstone deposits. The interpreted MDA for this unit is 110.2 ± 1.3, which is compatible with sample LP60 given their relative stratigraphic positions. Approximately, 64% of the ages are between 100 and 150 Ma and are represented in the primary peak at ca. 110 Ma with subordinate peaks at 130 and 143 Ma. Although arc magmatism began at ca. 150 Ma and was more or less continuous through the Cretaceous, episodes of peak magmatism are thought to have occured at 144–137, 136–127 and 126–75 Ma (Hervé *et al.*, 2007). Regardless of these intervals, based on detrital zircon signatures, the Cretaceous arc appears to be the primary source of detritus during the initial appearance of consistent sandstone deposition at LDLP. Additional, secondary peaks at ca. 270 and 520 Ma correspond closely to detrital signatures observed in the East Andean Metamorphic Complex (EAMC) (Hervé *et al.*, 2003) and are thus likely sourced by exhumation and recycling of the EAMC during early the depositional history of the MAB. Thus, detrital zircon provenance data from the LDLP outcrop are compatible with previous workers' interpretations of a westward thrust-belt source for early coarse clastic deposition in the MAB (Fildani *et al.*, 2003; McAtamney *et al.*, 2011).

Foreland basin development

In the well-constrained Magallanes Basin sector, the onset of foreland basin sedimentation is marked by an abrupt deepening of the basin (Natland *et al.*, 1974) and the appearance of consistent (deep water) coarse clastic deposition. We suggest that similar facies in the Austral Basin sector represent the same influences on basin evolution. Results from this study suggest a model whereby the onset of consistent, coarse clastic deposition is diachronously initiated from as far north as El Chalten, Argentina (*ca.* 49°S) to as far south as the Cordillera Darwin in Chile (*ca.* 54°S). This occurred in a time span of more than 10 Myr.

The southward younging trend observed in the initiation of coarse clastic deposition can be explained by one or a combination of the following end-member scenarios: (1) The MAB originated with a strong longitudinal sediment dispersal system from a northern point source and the delayed appearance of coarse clastics was a result of this sediment dispersal system slowly prograding southward. (2) Alternatively, the detritus for these deep-water fan systems is derived from more local, westward sources along smaller scale transverse dispersal systems that eventually feed into an overall axially drained deep-water basin (cf. Golo Fan, Gervais *et al.*, 2006). The second model would suggest that the diachronous appearance of coarse clastics was due to a progressive southward increase in sediment supply, which began sourcing these smaller, more localised tributaries that fed the deep-water fan system(s). Diachronous sediment supply could be achieved by increased uplift (and erosion) migrating southward possibly in response to along-strike (north to south) evolution of the sub-Andean fold and thrust belt. In short,

the first scenario invokes a point source model whereas the second scenario suggests more of a line source. Although it is beyond the scope of this study, one approach to resolving the feasibility of each of these models would be to compare provenance signatures between each of these outcrops as well as expected contributions from potential source areas.

It should be noted that our results depart from the Varela *et al.* (2012) interpretation of synchronous initiation of the basin in Chile and Argentina based on data from eastward prograding fluvial-estuarine deposits of the Mata Amarilla Formation (Figs 2 and 5), which began at *ca.* 100 Ma based on an interbedded tuff age of 96.2 ± 0.7 Ma collected from the middle Mata Amarilla Formation. Our alternative interpretation accounts for the timing and distribution of deep-marine facies gleaned from the new data presented in this study and is consistent with how previous models document this transition in the Chilean sector. For instance, our work suggests the presence of a deep-water basin (slope system) during the earliest Cenomanian in the Zona Centro region, which makes it difficult to reconcile having roughly coeval west-to-east progradation of shallow- to nonmarine depositional systems located to the east of the study area.

Paleogeographic implications

Submarine fan facies can be traced from as far south as the Cordillera Darwin in Chile to as far north as El Chalten, Argentina. In addition, we report new evidence for the existence of slope facies, which have not been previously documented for the early depositional history of the MAB. New constraints on the distribution of these facies as well as the timing of deposition provide a better understanding of the palaeogeography and initial basin fill during the early stages of the MAB (Fig. 19).

Late Aptian–Albian (115–100 Ma)

In the northern sector of the basin (*ca.* 49°S), the Aptian–Albian (as well as Cenomanian) time interval corresponds to an overall transition from rift-sag subsidence to retro-arc deformation and foreland basin development (Fig. 19). Consequently, there are also complexities in the range of depositional settings documented in different locations at this latitude. This study highlights the presence of high- and low-density turbidites interpreted as being deposited in an unconfined deep-marine environment. Based on U-Pb zircon geochronology, these deposits are late Aptian in age. Near Tres Lagos, approximately 100 km east of El Chalten, early Albian (Archangelsky *et al.*, 2008) fluvial-deltaic sequences have been identified as the Piedra Clavada Formation (Poire *et al.*, 2002). The tectonic context, provenance and spatial extent of both the turbiditic sandstone units from this study, as well as the Piedra Clavada Formation, remain largely unconstrained, making it difficult to assess the stratigraphic relationships between these two seemingly disparate units. On the basis of the data available at this time, we suggest that the deposition of deep-water turbidites documented in the Rio Mayer Formation (this study) not only predates deposition of the Piedra Clavada Formation but is also sufficiently distal to accommodate significant differences in depositional settings (e.g. fluvial deltaic vs. deep-water fan) (Fig. 19).

Cenomanian–Turonian (100–89 Ma)

Facies and architecture of earliest Cenomanian (or latest Albian) (*ca.* 100 Ma) documented at the ELH outcrop suggests that a southward-facing slope system was present in the Zona Centro region at this time. Ages of deep-water fan deposits in the vicinity of Lago Argentino may range from 93.7 to 100.4 Ma, based on 2σ uncertainties. Any direct relationships between these slope and fan systems during this time is difficult to determine, but should not be ruled out, as there is a subtle overlap in age, and a link between these systems would be consistent with the dominantly south-directed palaeocurrents documented in fan facies around Lago Argentino. In the northernmost part of the study area, this time interval corresponds to shallow-marine deposition of the Lago Viedma Formation (Arbe, 2002) near Cerro Pyramide (Figs 3 and 4) as well as shallow-marine and fluvial deposits of the Mata Amarilla Formation (Varela *et al.*, 2012) (Fig. 3). By the Turonian stage (*ca.* 92 Ma) the onset of fan deposition reached the Ultima Esperanza District of the Chilean sector of the basin, as suggested by detrital zircon maximum depositional ages (Fildani *et al.*, 2003).

Coniacian (89–85 Ma)

Based on maximum depositional ages of detrital zircon analyses, consistent deposition of medium-bedded sandstone (e.g. Lattore and upper La Panciencia Formations) near the latitude of Peninsula Brunswick (*ca.* 54°S) did not begin until at least 89 Ma and possibly not earlier than 85 Ma (McAtamney *et al.*, 2011) (Fig. 19). This represents the youngest known onset of deep-water fan deposition into the basin. The timing of these deposits corresponds to the early development of the Cerro Toro Formation (Figs 3 and 19), which includes the diachronous evolution of a well-documented sinuous axial channel belt in the Ultima Esperanza District (Hubbard *et al.*, 2008; Bernhardt *et al.*, 2012). Although these units are chronologically correlative, it is uncertain as to whether or not the deep-water fan system(s) in this portion of the basin were linked to the Cerro Toro channel belt to the north. Provenance interpretations by McAtamney *et al.* (2011) suggest a primarily westward (arc-derived) source.

Variations in crustal inheritance

The MAB and its predecessor Rocas Verdes Basin (RVB) represent a dynamic and long-lived (>150 Myr) history of tectonism. Previous studies have shown that inherited
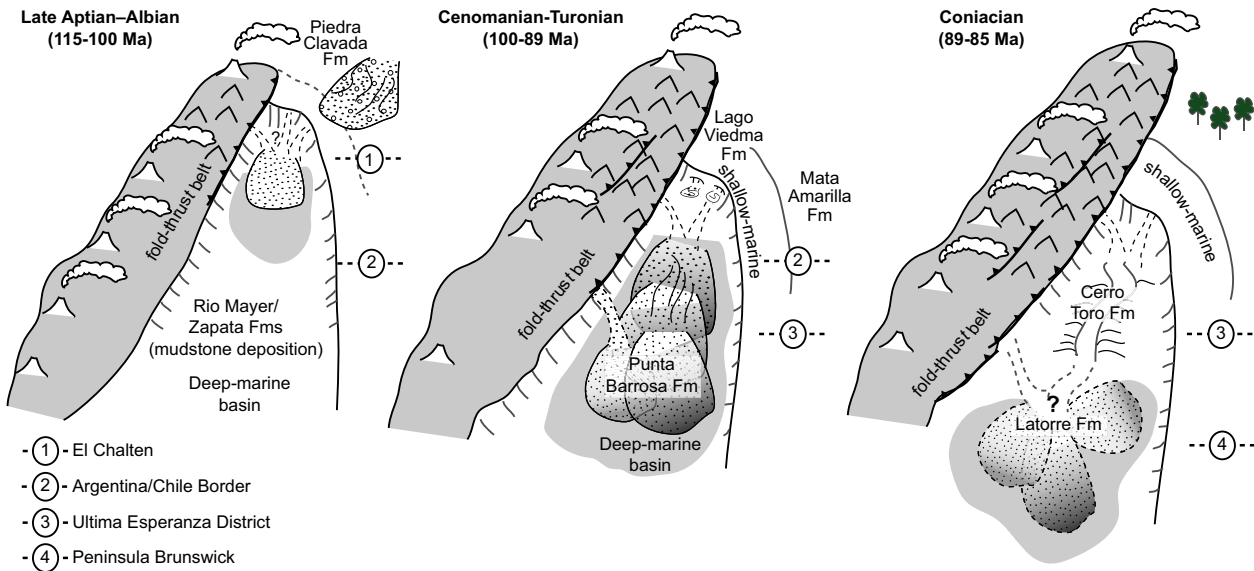
Fig. 19. Paleogeographic interpretations of the early fill of the MAB based on new results from this study and combined with previous workers' constraints from the Chilean basin sector (e.g. Fildani & Hessler, 2005; Romans *et al.*, 2010; McAtamney *et al.*, 2011; Fosdick *et al.*, 2014). See text for explanation. (a) Coarse clastic deposition of sediment gravity flows (e.g. LDLP section) had initiated in the northern basin sector (49°S) by late Aptian–Albian time while southern regions were characterised by dominantly fine-grained (mud) deposition; (b) By Cenomanian time (*ca.* 100 Ma) a deep-water slope system had developed near the latitude of Lago Viedma (e.g. ELH section) and during middle Cenomanian to earliest Turonian time (97–92 Ma) deposition along southward flowing deep-water fan system(s) characterised the early basin fill in regions between Lago Argentino and the Ultima Esperanza (UE) district of Chile (e.g. MP and BS sections); (c) Deposition of deep-water fan deposits initiated in the southern latitudes of the basin by Coniacian time, partially concurrent with deposition of the Cerro Toro Formation in the UE basin sector. It is unclear whether these deep-water systems were fed entirely from a northward point source or from more local (westward) source regions.

tectonics greatly influenced the structural and stratigraphic temporal evolution of the Magallanes Basin sector in Chile and highlight the differences between successor forelands such as the MAB and the commonly cited continental forelands in the Central Andes and North America (Fig. 1) (DeCelles & Giles, 1996; Horton & DeCelles, 1997; Romans *et al.*, 2010, 2011; Fosdick *et al.*, 2014). Within the sub-Andean region of southern Patagonia

(44°S–54°S), there are significant along-strike variations in the inherited crustal composition as a result of variations in the amount of extension during the rifting phase of the RVB (Fig. 20) (De Wit & Stern, 1981; Ramos *et al.*, 1982). This provides an excellent opportunity for assessing both the spatial and temporal effects that tectonic inheritance can impart on the stratigraphic evolution of a foreland basin.
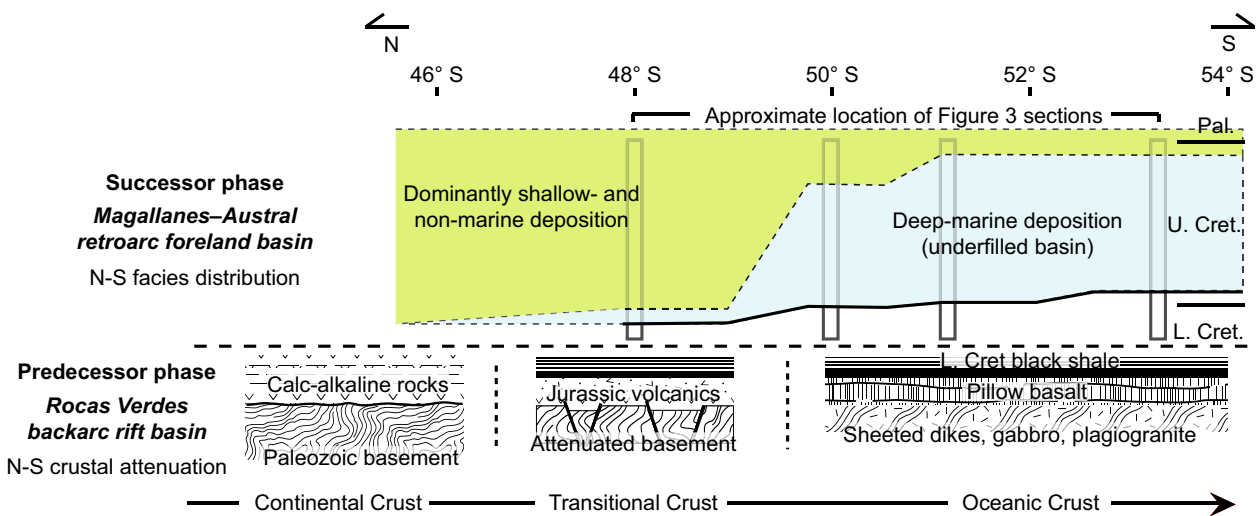

Fig. 20. Schematic diagram showing the spatial (north-to-south) relationship between crustal composition (Ramos *et al.*, 1982) as a result of the predecessor Rocas Verdes basin and the development and duration of deep- and shallow-marine depositional systems in the successor Magallanes–Austral foreland basin. Data sources same as in Fig. 3.

New geochronologic and facies relationships from this study offer better-constrained models for the early palaeogeography and stratigraphic evolution of the MAB (Fig. 3). Refined facies and chronostratigraphic relationships from different along-strike sectors of the basin reveal a distinct correlation between variations in crustal composition (from the preceding tectonic regime) and depositional setting (Fig. 20). That is, the majority of the Upper Cretaceous fill of the northern MAB consists of shallow- and nonmarine deposition where crustal compositions are continental and/or transitional (Fig. 20). However, further south in the basin where there was greater attenuation due to increased rifting and development of oceanic crust, nearly the entire Late Cretaceous phase of the basin is preserved by >4 km of deep-marine stratigraphy (Fig. 20). Furthermore, results from this study show that during the early (Albian–Cenomanian) evolution of the basin, the location of a deep-water slope setting was coincident with the transition from moderately attenuated 'transitional' crust to more greatly attenuate oceanic crust. In summary, these results support the notion that tectonic variations within a predecessor basin system can profoundly influence the spatial and temporal stratigraphic evolution of successor foreland basin systems.

SUMMARY AND CONCLUSIONS

Deep-water slope and/or fan deposits record the early depositional history of the MAB from as far north as El Chalten, Argentina (49°S) to at least as far south as the Cordillera Darwin (55°S). The stratigraphic architecture of the early fill of the Magallanes–Austral retroarc foreland basin is characterised by sediment gravity-flow deposits within a deep-water fan system with facies that range from a confined upper fan setting to distal lower fan and basin plain settings. Interpreted sediment gravity-flow processes include turbidity currents, debris flows and transitional flows with consistently southwest- to southeast-directed palaeoflow. Detailed stratigraphic sections and facies analysis from the Argentine sector of the MAB suggest that this fan system was overall progradational; however, lobe deposits along deep-water fan system(s) were unconfined and the basin margins likely did not influence the early stratigraphic architecture of the MAB. Thus, the progradational aspect of this system may have been governed more by sediment supply and source area uplift rather than the basin configuration and accommodation.

New zircon U–Pb ages from ash beds reveal a diachronous, southward younging trend in the onset of coarse clastic deposition into the basin. In the northernmost part of the study area (*ca.* 49°S), consistent sand deposition began as early as *ca.* 115 Ma; whereas in the southern basin sector (*ca.* 54°) significant coarse clastic deposition did not begin earlier than *ca.* 89–85 Ma. This progressive southward younging in the timing of consistent sand delivery into the basin is interpreted to reflect (1) gradual southward progradation of deep-water fan system from a northern point-source, and/or (2) southward increase and/or availability in local (likely westward) sediment supply in response to uplift and erosion associated with the southward migration and development of the sub-Andean fold-and-thrust belt. In either case, a dominantly axial (south-directed) sediment dispersal system was present during the early development of the basin. Finally, new constraints on the geochronology and facies of stratigraphy from the northern Austral Basin suggest that along-strike variations in the composition of inherited crust from the RVB phase may have profoundly influenced the long-term spatial distribution of depositional facies in the Upper Cretaceous MAB.

CONFLICT OF INTEREST

No conflict of interest declared.

SUPPORTING INFORMATION

Additional Supporting Information may be found in the online version of this article:

Appendix S1. Description of analytical methods in U–Pb zircon geochronology.
Appendix S2. Zircon U–Pb ash bed results.

REFERENCES

ANDERSON, K.S., GRAHAM, S.A. & HUBBARD, S.M. (2006) Facies, architecture, and origin of a reservoir-scale sand-rich succession within submarine canyon fill: insights from Wagon Caves Rock (Paleocene), Santa Lucia Range, California, USA. *J. Sediment. Res.*, **76**(5), 819–838.

ARBE, H.A. (2002) Análisis estratigráfico del Cretácico de la cuenca Austral (Stratigraphic analysis of the Cretaceous of the Austral Basin). Geologia y Recursos Naturales de Santa Cruz, Relatario del 15 Congreso Geológico Argentino, 103–128.

ARBE, H.A. & HECHEM, J.J. (1984) Estratigrafía y facies de depósitos marinos profundos del Cretácico superior, Lago Argentino, pp. 7–41. Provincia de Santa Cruz. IX Congreso Geológico Argentino, Actas V.

ARCHANGELSKY, A., ARCHANGELSKY, S., POIRÉ, D.G. & CANESSA, N.D. (2008) Registros palinológicos en la Formación Piedra Clavada (Albiano) en su área tipo, provincia de Santa Cruz, Argentina. *Revista del Museo Argentino de Ciencias Naturales*, **10**, 185–198.

ARMENTROUT, J.M., KANSCHAT, K.A., MEISLING, K.E., TSAKMA, J.J., ANTRIM, L. & McCONNELL, D.R. (2000) AAPG Memoir 72/SEPM Special Publication No. 68, Chapter 9: Neogene Turbidite Systems of the Gulf of Guinea Continental Margin Slope, Offshore Nigeria.

ARMITAGE, D.A., ROMANS, B.W., COVAULT, J.A. & GRAHAM, S.A. (2009) The influence of mass transport deposit topography on the evolution of turbidite architecture: The Sierra Contreras, Tres Pasos Formation (Cretaceous), southern Chile. *J. Sediment. Res.*, **79**, 287–301.

BEAUMONT, C. (1981) Foreland basins. *Geophys. J. Int.*, **65**(2), 291–329.

BERNHARDT, A., JOBE, Z., GROVE, M. & LOWE, D. (2012) Paleogeography and diachronous infill and of an ancient deep-marine Foreland Basin, Upper Cretaceous Cerro Toro Formation, Magallanes Basin. *Basin Res.*, **23**, 1–26.

BIDDLE, K.T., ULIANA, M.A., MITCHUM, R.M. Jr., FITZGERALD, M.G. & WRIGHT, R.C. (1986) The stratigraphic and structural evolution of the central and eastern Magallanes Basin, southern South America. In: *Foreland Basins* (Ed. by Allen P.A. & Homewood P.) *International Association of Sedimentologists Spec. Publ.*, **8**, 41–61.

BOUMA, A.H. (1962) *Sedimentology of Some Flysch Deposits*. Elsevier, Amsterdam. p. 168.

CALDERÓN, M., FILDANI, A., HERVÉ, F., FANNING, C.M., WEISLOGEL, A. & CORDANI, U. (2007) Late Jurassic bimodal magmatism in the northern sea-floor remnant of the Rocas Verdes basin, southern Patagonian Andes. *J. Geol. Soc. London*, **164**, 1011–1022.

CORTÉS, R. (1964) Estratigrafía y un estudio de paleocorrientes del flysch Cretáceo del Depto. de Ultima Esperanza, p. S117. Tesis de grado, Universidad Técnica de Estado, Santiago, Chile.

COVAULT, J.A., ROMANS, B.W. & GRAHAM, S.A. (2009) Outcrop expression of a continental-margin-scale shelf-edge delta from the Cretaceous Magallanes Basin, Chile. *J. Sediment. Res.*, **79**, 523–539.

CRANE, W.H. & LOWE, D.R. (2008) Architecture and evolution of the Paine channel complex, Cerro Toro Formation (Upper Cretaceous), Silla Syncline, Magallanes Basin, Chile. *Sedimentology*, **55**, 979–1009.

DALZIEL, I.W.D., de WIT, M.J. & PALMER, K.F. (1974) Fossil marginal basin in the southern Andes. *Nature*, **250**, 291–294.

DE RUIG, M.J. & HUBBARD, S.M. (2006) Seismic facies and reservoir characteristics of a deep-marine channel belt in the Molasse foreland basin, Puchkirchen Formation, Austria. *AAPG Bulletin*, **90**, 735–752.

DE WIT, M.J. & STERN, C.R. (1981) Variations in the degree of crustal extension during formation of a back-arc basin. *Tectonophysics*, **72**, 229–260.

DECELLES, P.G. & GILES, K.A. (1996) Foreland basin systems. *Basin Res.*, **8**(2), 105–123.

DESEGAULX, P., KOOI, H. & CLOETINGH, S. (1991) Consequences of foreland basin development on thinned continental lithosphere: application to the Aquitaine basin (SW France). *Earth Planet. Sci. Lett.*, **106**(1), 116–132.

DICKINSON, W.R. (1974) Plate tectonics and sedimentation. *Spec. Publ. SEPM*, **22**, 1–27.

FILDANI, A. & HESSLER, A.M. (2005) Stratigraphic record across a retroarc basin inversion: Rocas Verdes-Magallanes Basin, Patagonian Andes, Chile. *GSA Bulletin*, **117**, 1596–1614.

FILDANI, A., COPE, T.D., GRAHAM, S.A. & WOODEN, J.L. (2003) Initiation of the magallanes foreland basin: timing of the southernmost Patagonian Andes orogeny revised by detrital zircon provenance analysis. *Geology*, **31**, 1081–1084.

FILDANI, A., CRANE, W.H., ROMANS, B.W., HUBBARD, S.M. & SHULTZ, M.R. (2007) Mesozoic through early tertiary stratigraphic evolution and deep-water deposition of the Magallanes Basin, Chile. *AAPG Bulletin*, **47**, 506–524.

FOSDICK, J.C., ROMANS, B.W., FILDANI, A., BERNHARDT, A., CALDERÓN, M. & GRAHAM, S.A. (2011) Kinematic evolution of the Patagonian retroarc fold- and-thrust belt and Magallanes foreland basin, Chile and Argentina, 51°30′S. *GSA Bulletin*, **123**, 1679–1698.

FOSDICK, J.C., GRAHAM, S.A. & HILLEY, G.E. (2014) Influence of attenuated lithosphere and sediment loading on flexure of the deep-water Magallanes retroarc foreland basin, Southern Andes. *Tectonics*, **33**, 1–21.

GALLOWAY, W.E. (1998) Siliciclastic slope and base-of-slope depositional systems: component facies, stratigraphic architecture, and classification. *AAPG Bulletin*, **82**(4), 569–595.

GARDNER, M. (1995) The stratigraphic hierarchy and tectonic history of the mid-cretaceous foreland basin of central Utah. *Spec. Publ. SEPM*, **52**, 283–303.

GERVAIS, A., SAVOYE, B., MULDER, T. & GONTHIER, E. (2006) Sandy modern turbidite lobes: a new insight from high resolution seismic data. *Marine Petrol. Geol.*, **23**(4), 485–502.

GHIGLIONE, M.C., SUAREZ, F., AMBROSIO, A., DA POIAN, G., CRISTALLINI, E.O., PIZZIO, M.F. & REINOSO, R.M. (2009) Structure and evolution of the Austral Basin fold-thrust belt, southern Patagonian Andes. *Revista de la Asociación Geológica Argentina*, **65**, 215–226.

GHOSH, B. & LOWE, D.R. (1993) *The Architecture of Deep-Water Channel Complexes*, pp. 51–65. Cretaceous Venado sandstone Member, Sacramento valley, CA.

GRAHAM, S.A., HENDRIX, M.S., WANG, L.B. & CARROLL, A.R. (1993) Collisional successor basins of western China: impact of tectonic inheritance on sand composition. *Geol. Soc. Am. Bullet.*, **105**(3), 323–344.

HAUGHTON, P.D., BARKER, S.P. & McCAFFREY, W.D. (2003) 'Linked'debrites in sand-rich turbidite systems–origin and significance. *Sedimentology*, **50**(3), 459–482.

HAUGHTON, P., DAVIS, C., McCAFFREY, W. & BARKER, S. (2009) Hybrid sediment gravity flow deposits – classification, origin and significance. *Marine Petrol. Geol.*, **26**, 1900–1918.

HELLER, P.L., ANGEVINE, C.L., WINSLOW, N.S. & PAOLA, C. (1988) Two-phase stratigraphic model of foreland-basin sequences. *Geology*, **16**(6), 501–504.

HERVÉ, F., FANNING, C. & PANKHURST, R. (2003) Detrital zircon age patterns and provenance of the metamorphic complexes of southern Chile. *J. South Am. Earth Sci.*, **16**, 107–123.

HERVÉ, F., PANKHURST, R.J., FANNING, C.M., CALDERÓN, M. & YAXLEY, G.M. (2007) The South Patagonian batholith: 150 my of granite magmatism on a plate margin. *Lithos*, **97**(3), 373–394.

HODGSON, D.M. (2009) Distribution and origin of hybrid beds in sand-rich submarine fans of the Tanqua depocentre, Karoo Basin, South Africa. *Marine Petrol. Geol.*, **26**(10), 1940–1956.

HORTON, B.K. & DECELLES, P.G. (1997) The modern foreland basin system adjacent to the Central Andes. *Geology*, **25**(10), 895–898.

HOWELL, D.G. & NORMARK, W.R. (1982) Sedimentology of submarine fans. Sandstone Depositional Environments. *Am. Associat. Petrol. Geolog. Memoir*, **31**, 365–404.

HUBBARD, S.M., ROMANS, B.W. & GRAHAM, S.A. (2008) Deep-water foreland basin deposits of the Cerro Toro Formation, Magallanes Basin, Chile: architectural elements of a sinuous basin axial channel belt. *Sedimentology*, **55**, 1333–1359.

IMBER, J., CHILDS, C., NELL, P.A.R., WALSH, J.J., HODGETTS, D. & FLINT, S. (2003) Hanging wall fault kinematics and footwall collapse in listric growth fault systems. *J. Struct. Geol.*, **25**(2), 197–208.

JOBE, Z.R., BERNHARDT, A. & LOWE, D.R. (2010) Facies and architectural asymmetry in a conglomerate-rich submarine channel fill, Cerro Toro Formation, Sierra del Toro, Magallanes Basin, Chile. *J. Sediment. Res.*, **80**, 1085–1108.

JORDAN, T.E. (1995) Retroarc foreland and related basin. In: *Tectonics of Sedimentary Basins* (Ed. by C.J. Busby, R.V. Ingersoll), pp. 331–362. Blackwell Science, Oxford.

KATZ, H.R. (1963) Revision of cretaceous stratigraphy in Patagonian Cordillera of Ultima Esperanza, Magallanes Province, Chile. *Am. Associat. Petrol. Geol. Bullet.*, **47**, 506–524.

KOSMAL, A. & SPIKERMANN, J.P. (2001) Geología de la zona del Cerro Fitz Roy, Provincia de Santa Cruz. *Rev. Mus. Argent. Cienc. Nat.*, **3**(1), 41–53.

KRAEMER, P.E. & RICCARDI, A.C. (1997) Estratigrafía de la region comprendida entre los lagos Argentino y Viedma (49°40′–50°10′ lat. S), Provincia de Santa Cruz. *Revista de la Asociación Geológica Argentina*, **52**, 333–360.

LEIER, A.L., DECELLES, P.G., KAPP, P. & DING, L. (2007) The Takena Formation of the Lhasa terrane, southern Tibet: The record of a Late Cretaceous retroarc foreland basin. *Geol. Soc. Am. Bullet.*, **119**(1–2), 31–48.

LOWE, D.R. (1982) Sediment gravity flows: II. depositional models with special reference to the deposits of high-density turbidity currents. *J. Sediment. Petrol.*, **52**, 0279–0297.

LOWE, D.R. & GHOSH, B. (2004) A stratigraphic and architectural-element methodology for the subdivision and interpretation of deep-water clastic sequences: an example from the Cretaceous Venado Sandstone, Sacramento Valley, California. Deep-Water Sedimentation: Technological Challenges for the Next Millennium: Brazilian Association of Petroleum Geologists, Special Paper, 42–56.

LOWE, D.R. & GUY, M. (2000) Slurry-flow deposits in the Britannia Formation (Lower Cretaceous), North Sea: a new perspective on the turbidity current and debris Flow problem. *Sedimentology*, **47**, 31–70.

MACEACHERN, J.A., PEMBERTON, S.G., GINGRAS, M.K. & BANN, K.L. (2010) Ichnology and facies models. In: *Facies Models 4, Geological Association of Canada* (Ed. by M.P. James & R.W. Dalrymple), pp. 19–58. GEOtext 6, ISSN 1208-2260.

MAHON, K.I. (1996) The New "York" regression: application of an improved statistical method to geochemistry. *Int. Geol. Rev.*, **38**(4), 293–303.

MCATAMNEY, J., KLEPEIS, K., MEHRTENS, C., THOMSON, S., BETKA, P., ROJAS, L. & SNYDER, S. (2011) Along-strike variability of back-arc basin collapse and the initiation of sedimentation in the Magallanes foreland basin, southernmost Andes (53–54.5°S). *Tectonics*, **30**(5).

MPODOZIS, C., ALVAREZ, P., ELGUETA, S., MELLA, P., HERVÉ, F. & FANNING, M. (2007) Revised Cretaceous stratigraphy of the Magallanes Foreland Basin at Seno Skyring: Regional implications of new SHRIMP age data on detrital zircon populations, paper presented at GEOSUR 2007 International Congress on the Geology and Geophysics of the Southern Hemisphere, Univ. Católica de Chile, Santiago, 20–21 Nov.

MUTTI, E. (1977) Distinctive thin-bedded turbidite facies and related depositional environments in the Eocene Hecho Group (South-central Pyrenees, Spain). *Sedimentology*, **24**, 107–131.

MUTTI, E. & NORMARK, W.R. (1987) Comparing examples of modern and ancient turbidite systems: problems and concepts. In: *Marine Clastic Sedimentology* (Eds. K.J. Myers & P.B. Wignall), pp. 1–38. Springer, the Netherlands.

MUTTI, E. & RICCI LUCHI, F. (1975) Turbidite facies and facies associations. In: *Examples of Turbidite Facies and Facies Associations From Selected Formations of the Northern Apennines* (Ed. by E. Mutti, G.C. Parea, F. Ricci Lucchi, M. Sagri, G. Zanzucchi, G. Ghibaudo & S. Jaccarino), pp. 21–36, IX Int. Congr. Sedim. Nice 75, Field Trip A 11.

MUTTI, E., NILSEN, T.H. & RICCI LUCHI, F. (1978) Outer fan depositional lobes of the Laga Formation (upper Miocene and lower Pliocene), east-central Italy. In: *Sedimentation in Submarine Canyons, Fans and Trenches*, pp. 210–223.

NATLAND, M.L., EDUARDO, G.P., CAÑON, A. & ERNST, M. (1974) A system of stages for correlation of Magallanes Basin sediments. *Geol. Soc. Am. Memoirs*, **139**, 1–126.

NORMARK, W.R. (1978) Fan valleys, channels, and depositional lobes on modern submarine fans: characters for recognition of sandy turbidite environments. *AAPG Bulletin*, **62**(6), 912–931.

PANKHURST, R.J., RILEY, T.R., FANNING, C.M. & KELLEY, S.P. (2000) Episodic silicic volcanism in Patagonia and the Antarctic Peninsula: Chronology of magmatism associated with the break-up of Gondwana. *J. Petrol.*, **41**, 605–625.

PICKERING, K., STOW, D., WATSON, M. & HISCOTT, R. (1986) Deep-water facies, processes and models: a review and classification scheme for modern and ancient sediments. *Earth-Sci. Rev.*, **23**(2), 75–174.

PIPER, D.J. & NORMARK, W.R. (1983) Turbidite depositional patterns and flow characteristics, Navy submarine fan, California Borderland. *Sedimentology*, **30**(5), 681–694.

POIRE, D.G., CANESSA, N.D., CARLONI, A. & FERRER, O. (2002) La Formación Piedra Clavada en el área de Tres Lagos, provincia de Santa Cruz, Argentina. In: *XV Congreso Geológico Argentino* (El Calafate, Santa Cruz), Actas, p. 6.

POSAMENTIER, H.W. & MARTINSEN, O.J. (2011) The character and genesis of submarine mass-transport deposits: insights

from outcrop and 3D seismic data. Mass-transport deposits in deepwater settings. *SEPM Spec. Publ.*, 96, 7–38.

PRATHER, B.E., BOOTH, J.R., STEFFENS, G.S. & CRAIG, P.A. (1998) Classification, lithologic calibration, and stratigraphic succession of seismic facies of intraslope basins, deep-water Gulf of Mexico. *AAPG bulletin*, 82(5), 701–728.

PRELAT, A., COVAULT, J.A., HODGSON, D.M., FILDANI, A. & FLINT, S.S. (2010) Intrinsic controls on the range of volumes, morphologies, and dimensions of submarine lobes. *Sed. Geol.*, 232(1), 66–76.

PRÉLAT, A., HODGSON, D.M. & FLINT, S.S. (2009) Evolution, architecture and hierarchy of distributary deep-water deposits: a high-resolution outcrop investigation from the Permian Karoo Basin, South Africa. *Sedimentology*, 56, 2132–2154.

PUIGDEFÀBREGAS, C., MUÑOZ, J.A. & VERGÉS, J. (1992). Thrusting and foreland basin evolution in the southern Pyrenees. In: *Thrust Tectonics* (Eds. J.A. Muñoz & K. McClay), pp. 247–254. Springer, the Netherlands.

RAMOS, V.A., NIEMEYER, H., SKARMETA, J. & MUÑOZ, J. (1982) Magmatic evolution of the Austral Patagonian Andes. *Earth Sci. Rev.*, 18, 411–443.

RICCI LUCCHI, F. (1975) Depositional cycles in two turbidite formations of northern Apennines. *J. Sediment. Res.*, 45(1), 3–43.

RICHIANO, S. (2014) Lower Cretaceous anoxic conditions in the Austral basin, south-western Gondwana, Patagonia Argentina. *J. South Am. Earth Sci.*, 54, 37–46.

ROMANS, B.W., HUBBARD, S.M. & GRAHAM, S.A. (2009) Stratigraphic evolution of an outcropping continental slope system, Tres Pasos formation at Cerro Divisadero, Chile. *Sedimentology*, 56, 737–764.

ROMANS, B.W., FILDANI, A., GRAHAM, S.A., HUBBARD, S.M. & COVAULT, J.A. (2010) Importance of predecessor basin history on sedimentary fill of a retroarc foreland basin: provenance analysis of the Creceous Magallanes Basin, Chile. *Basin Res.*, 22, 640–658.

ROMANS, B.W., FILDANI, A., HUBBARD, S.M., COVAULT, J.A., FOSDICK, J.C. & GRAHAM, S.A. (2011) Evolution of deep-water stratigraphic architecture, Magallanes Basin, Chile. *Marine Petrol. Geol.*, 28, 612–628.

SAUNDERS, A.D., TARNEY, J., STERN, C.R. & DALZIEL, I.W.D. (1979) Geochemistry of Mesozoic marginal basin-floor igneous rocks from southern Chile. *GSA Bulletin*, 90, 237–258.

SCHULTZ, M.R., FILDANI, A., COPE, T.A. & GRAHAM, S.A. (2005). Deposition and stratigraphic architecture of an outcropping ancient slope system: Tres Pasos formation, Magallanes Basin, southern Chile. In: *Submarine Slope Systems: Processes and Products* (Ed. by Hodgson D.M.& Flint S.S.) *Geological Society of London, Spec. Publ.* 244, 27–50.

SCHWANS, P. (1995) Controls on sequence stacking and fluvial to shallow-marine architecture in a foreland basin, AAPG Special Volume, 64.

SCHWARTZ, T.M. & GRAHAM, S.A. (2014) Stratigraphic architecture of a tide influenced shelf edge delta, Upper Cretaceous Dorotea Formation, Magallanes Austral Basin, Patagonia. *Sedimentology*, 62, 1039–1077.

SHIPP, R.C., WEIMER, P. & POSAMENTIER, H.W. (Eds.). (2011) Mass-transport deposits in deepwater settings (No. 96).

SEPM Soc. Sed. Geol., pp. 3–6. SEPM special publication 96, Tulsa, Oklahoma.

SHULTZ, M.R. & HUBBARD, S.M. (2005) Sedimentology, Stratigraphic Architecture, and Ichnology of Gravity-Flow Deposits Partially Ponded in a Growth-Fault-Controlled Slope Minibasin, Tres Pasos Formation (Cretaceous), Southern Chile. *Journal of Sedimentary Research*, 75, 440–453.

STOCKMAL, G.S., BEAUMONT, C. & BOUTILIER, R. (1986) Geodynamic models of convergent margin tectonics: transition from rifted margin to overthrust belt and consequences for foreland-basin development. *AAPG Bulletin*, 70(2), 181–190.

SZWARC, T.S., JOHNSON, C.L., STRIGHT, L.E. & MCFARLANE, C.M. (2014) Interactions between axial and transverse drainage systems in the Late Cretaceous Cordilleran foreland basin: evidence from detrital zircons in the Straight Cliffs Formation, southern Utah, USA. *GSA Bulletin*, 127, 372–392.

TALLING, P.J. (2013) Hybrid submarine flows comprising turbidity current and cohesive debris flow: deposits, theoretical and experimental analyses, and generalized models. *Geosphere*, 9(3), 460–488.

Van der MERWE, W.C., HODGSON, D.M., BRUNT, R.L. & FLINT, S.S. (2014) Depositional architecture of sand-attached and sand-detached channel-lobe transition zones on an exhumed stepped slope mapped over a 2500 km^2 area. *Geosphere*, 10(6), 1076–1093.

VARELA, A.N., POIRÉ, D.G., MARTIN, T., GERDES, A., GOIN, F.J., GELFO, J.N. & HOFFMANN, S. (2012) U–Pb zircon constraints on the age of the Cretaceous Mata Amarilla Formation, Southern Patagonia, Argentina: its relationship with the evolution of the Austral Basin. *Andean Geol.*, 39(3), 359–379.

VARELA, A.N., GÓMEZ-PERAL, L.E., RICHIANO, S. & POIRÉ, D.G. (2013) Distinguishing similar volcanic source areas from an integrated provenance analysis: implications for Foreland Andean Basins. *J. Sediment. Res.*, 83(3), 258–276.

WALKER, R.G. (1978) Deep-water sandstone facies and ancient submarine fans: models for exploration for stratigraphic traps. *AAPG Bulletin*, 62(6), 932–966.

WANG, C., SCOTT, R.W., WAN, X., GRAHAM, S.A., HUANG, Y., WANG, P., WU, H., DEAN, W.E. & ZHANG, L (2013) Late Cretaceous climate changes recorded in eastern Asian lacustrine deposits and North American epieric sea strata. *Earth Sci. Rev.*, 126, 300–320.

WILSON, T.J. (1991) Transition from back-arc to foreland basin development in the southernmost Andes: stratigraphic record from the Ultima Esperanza District, Chile. *Geol. Soc. Am. Bulletin*, 103, 98–115.

WINN, R.D. & DOTT, R.H. Jr (1979) Deep-water fan-channel conglomerates of Late Cretaceous age, southern Chile. *Sedimentology*, 26, 203–228.

WYNN, R.B., KENYON, N.H., MASSON, D.G., STOW, D.A. & WEAVER, P.P. (2002) Characterization and recognition of deep-water channel-lobe transition zones. *AAPG Bulletin*, 86(8) 1441–1462.